5-2009

Modeling and analysis of proximal tibial growth plate fractures in adolescents

Susan Ann Basile
University of Tennessee

To the Graduate Council:

I am submitting herewith a thesis written by Susan Ann Basile entitled "Modeling and analysis of proximal tibial growth plate fractures in adolescents." I have examined the final electronic copy of this thesis for form and content and recommend that it be accepted in partial fulfillment of the requirements for the degree of Master of Science, with a major in Biomedical Engineering.

Xiaopeng Zhao, Major Professor

We have read this thesis and recommend its acceptance:

Accepted for the Council:
Carolyn R. Hodges

Vice Provost and Dean of the Graduate School

(Original signatures are on file with official student records.)

To the Graduate Council:

I am submitting herewith a thesis written by Susan Ann Basile entitled “Modeling and Analysis of Proximal Tibial Growth Plate Fractures in Adolescents”. I have examined the final electronic copy of this thesis for form and content and recommend that it be accepted in partial fulfillment of the requirements for the degree of Master of Science, with a major in Biomedical Engineering.

Xiaopeng Zhao
Major Professor

We have read this thesis
and recommend its acceptance:

Clare Milner

Mingjun Zhang

Accepted for the Council:

Carolyn R. Hodges
Vice Provost and
Dean of the Graduate School

(Original signatures are on file with official student records)

Modeling and Analysis of Proximal Tibial Growth Plate Fractures in Adolescents

A Thesis

Presented for the

Master of Science

Degree

The University of Tennessee, Knoxville

Susan Ann Basile

May 2009

For Kathy - who from the day we met believed in me more than I ever believed in myself.

ACKNOWLEDGEMENTS

A special thank you and acknowledgement to Mr. James Pippin and the Pipeline Engineering Diversity Fellowship program, for their tremendous generosity. Without their emotional and financial support, I I don't know if I would have been able to see my graduate studies at the University of Tennessee to fruition.

My sincerest thanks to my advisor Dr. Xiaopeng Zhao for his support and leadership. I am grateful for his straightforward and honest advice, his willingness to push me out of my intellectual comfort zone and think more deeply, as well as his confidence in both me and my work.

I also extend gratitude to my thesis committee – Dr. Claire Milner and Dr. Mingjun Zhang - for their instruction in the classroom, and their advice out of it. My thanks to both for their time and contributions.

I collectively show love and thanks to my family and friends, whom are a never-ending source of love, support, advice, and perhaps most importantly, understanding and patience.

ABSTRACT

Today, children and adolescents are participating heavily in organized athletics year-round. Each year, approximately one third of these children will experience a serious injury requiring a doctor's or hospital visit. A large number of these are overuse injuries. Physeal, or growth plate fractures, are one such type of overuse injury commonly seen in adolescents. At the knee joint, overuse injuries in adolescents occur most often in the proximal region of the tibia. Conversely, in mature adults, overuse injuries manifest themselves more often at the middle/distal third junction of the tibia, or in the soft tissues of the knee joint. While the exact reasons for this difference have not been directly and definitively quantified, several hypotheses have been suggested. They include differences in mechanical movement strategies, changes in limb inertial and material properties, and the timing of these changes in relation to one another. In addition, the presence of an inherently weaker growth plate is present throughout growth, since the growth plate is the last portion of the bone to ossify. This renders the epiphyseal and metaphyseal; areas more susceptible to injury than the than the diaphysis, and loads that would typically cause damage or rupture to soft tissues like the ACL or MCL instead disrupt the weaker physeal plate. This thesis aims to compare the changes in and interaction of inertial properties and forces produced by the quadriceps via the patellar tendon and tibiofemoral contact before and after puberty. To this end, these forces were first determined using Kane's method of dynamics in conjunction with an isometric knee extension study yielding separate adult and youth data. These results were then utilized in the finite element software package Abaqus to load tibial models with varying material properties and investigate changes in stress and strain at the proximal tibia. Shortened patellar ligament and increased force at the ankle had the greatest effect on forces at the proximal tibia. The areas at greatest risk for fracture from the finite element analysis were the posterior and lateral/medial portions of the metaphysis.

TABLE OF CONTENTS

Chapter **Page**

CHAPTER I: INTRODUCTION....1
Background and General Information....1
Clinical Relevance....4
Problem Statement....4
CHAPTER II: LITERATURE REVIEW....5
2.1 Anatomy....5
2.1.1 Growth Plate Anatomy & Long Bone Growth....5
2.1.2 Fracture Classifications....6
2.1.3 Transformations in Bone and Muscle Properties....6
2.2 Youth Athletics and Injury....12
2.2.1 Case Studies....12
2.3 Experiments....14
2.3.1 Failure Modes of Epiphyseal Plate Cartilage....14
2.3.2 Tensile Properties of Bovine Physis....15
2.4 Computational Methods....15
2.4.1 Mathematical Modeling....16
2.5 Finite Element Analysis....17
2.5.1 Slipped Capital Femoral Epiphysis....18
2.5.2 Pediatric Lumbar Spine....19
CHAPTER III: MATHEMATICAL MODELING AND INVERSE DYNAMICS....20
3.1 Introduction....20
3.2 Leg Extension Model....21
3.3 Results....25
3.3.1 Age Comparison....25
3.3.2 Individual Factor Comparison....34
CHAPTER IV: FINITE ELEMENT ANALYSIS....41
4.1 Assumptions....41
4.2 Model Description....42
4.2.1 Material Properties....42

4.2.2 Loading Conditions 43
4.3 Results 44
4.3.1 von Mises Stresses 44
4.3.2 Strain and Shear Stress 47
4.3.3 Viscoelastic Comparison 47
4.3.4 Jump Take-Off Comparison 47
4.4 Summary 54
CHAPTER V: FUTURE CONSIDERATIONS AND CONCLUSIONS 55
5.1 Mathematical Model 55
5.2 FE Model 56
5.3 Future Considerations 56
5.4 Conclusions 57
REFERENCES 58
APPENDICES 64
Appendix A. Autolev Codes, Outputs, and Graphs 65
A.1 Autolev Code (adult with dynamometer force) 65
A.2 Autolev Output File (13 year-old) 69
A.3 Fortan code for the slow adult model 75
A.4 Matlab code for the slow 13 year-old model. 83
Appendix B. Abaqus Contour Images 95
VITA 97

LIST OF TABLES

Table 1. Salter-Harris Classifications of Epiphyseal Fractures (Wheeless 1996).....7
Table 2. Proximal tibial fracture data (Laor, Wall et al. 2006). 13
Table 3. Body segment parameters (Jensen 1989). 24
Table 4. Average values used for youth and adult Autolev models. The force is the dynamometer force at the ankle, at the various constant speeds (Kanehisa, Yata et al. 1995). 24
Table 5. Property values for the factor comparison Autolev codes. 25
Table 6. Young's and shear moduli used in Abaqus simulation. Values are in MPa. ..43
Table 7. Contents of 13_fast.2 - Normal and shear femorotibial forces for fast extension adolescent model. 91
Table 8. Contents of fast_grf.2 - Normal and shear femorotibial forces for jump take-off model. 92
Table 9. Contents of 13_fast.3 - Patellar tendon force for the fast extension model, separated into its components 93
Table 10. Contents of fast_grf.3 - Patellar tendon force for jump take-off model, separated into components. 94

LIST OF FIGURES

Figure 1. Depiction of Growth Plate Layers (Radhakrishnan, Lewis et al. 2004).....7
Figure 2. Salter-Harris Classifications. 'M' designates that the fracture runs through the metaphysis, and 'E' designates that it runs through the epiphysis. 8
Figure 3. Lateral view of a type 3 fracture with mild posterior displacement of the epiphysis and widening of the metaphysis. Subject was a fifteen year-old boy injured preparing to take off from a jump while playing basketball (Peterson 2007). 9
Figure 4. Eleven year-old tennis player who refused treatment or rest for bilateral physeal fractures of the proximal tibia. Note the varus alignment (*left*) six years after diagnosis. (Laor, Wall et al. 2006).....13
Figure 5. Finite element modeling flowchart (www.biomesh.org).....17
Figure 6. Femorotibial points and frames. NA - contact point on the femur, AN - contact point on the tibia, AC – distal end of the tibia, AO – center of mass of the tibia, ANAC – length of the tibia, AOAC – distance from the CoM to the distal end of the tibia. 26
Figure 7. Patellar Tendon/Tibial points and frames. AB – Patellar tendon insertion point, BO – midway point of patellar ligament, ANAB1, ANAB2 – distance from the proximal end of the tibia to the patellar ligament insertion point in the A1> and A2> directions. 27
Figure 8. Forces acting on the tibia during an isometric leg extension. FNA1, FNA2 – femorotibial shear and normal forces, FAB – patellar ligament tensile force, F_D – dynamometer force acting at the distal end of the tibia, FOOT – weight of the foot. 28
Figure 9. Animation snapshots of adult Autolev code at t = .10 and t = .75 seconds. ..29
Figure 10. Age related change in patellar ligament force at 1.05 radians per second .30
Figure 11. Age related changes in tibiofemoral shear force at 1.05 radians per second 31
Figure 12. Age related changes in femorotibial normal force at 1.05 radians per second. 32
Figure 13. Age related change in patellar ligament force at 3.14 radians per second. Normalized forces can be found in the appendix. 33

Figure 14. Factor related change in patellar ligament force at 1.05 radians per second. 36
Figure 15. Factor related change in patellar ligament force at 3.14 radians per second. 37
Figure 16. Factor related changes in tibial shear force at 1.05 radians per second. ...38
Figure 17. Factor related change in femorotibial normal force at 1.05 radians per second. 39
Figure 18. Factor related change in femorotibial normal force at 3.14 radians per second. 40
Figure 19. Posterior (top) and anterior views of von Mises stress contour plots on transversely isotropic growth plate model.....45
Figure 20. Posterior (top) and anterior views of mises stress contour plots for the stronger transversely isotropic model (no growth plate). 46
Figure 21. Impingement of popliteal artery from fractured physis (Peterson 2007). 48
Figure 22. Posterior strain in the transversely isotropic growth plate (top) and stronger models. Contours of anterior strain are located in the appendix. 49
Figure 23. Vector representation of maximum (red) and minimum (blue) principal stresses. 50
Figure 24. Viscoelastic model posterior stress (top) and anterior strain. Contours of anterior stress and posterior strain are located in the append 51
Figure 25. Jump take-off anterior (top) and posterior mises stress. 52
Figure 26. Jump take-off anterior (top) and posterior strain. 53
Figure 27. Age related changes in normalized patellar ligament force at 3.14 rad/s. ...88
Figure 28. Age related changes in normalized femorotibial normal force at 3.14 rad/s. 89
Figure 29. Age related changes in normalized femorotibial shear force at 3.14 rad/s. .90
Figure 30. Anterior strain in the transversely isotropic growth plate model (top) and stronger material model. 95
Figure 31. Viscoelastic model anterior stress (top) and posterior strain. 96

LIST OF ABBREVIATIONS

BMI	Body Mass Index
BW	Body Weight
CSA	Cross-Sectional Area
E_{ij}	Young's Modulus
FEA	Finite Element Analysis
G_{ij}	Shear Modulus
GRF	Ground Reaction Force
SCFE	Slipped Capital Femoral Epiphysis
VGRF	Vertical Ground Reaction Forces
ν_{ij}	Poisson's Ratio

CHAPTER I: INTRODUCTION

Background and General Information

Current estimates assert that 30 to 45 million American children participate in at least one organized athletic activity. Every year, about one third of these young people will encounter an injury that necessitates a visit to a medical professional, resulting in yearly healthcare costs of up to $1.8 billion (Adirim and Cheng 2003). Overuse – repetitive micro trauma to a tendon, bone, or joint without adequate regeneration or healing time - contributes to up to half of these injuries (Dalton 1992).

Today, more children are participating in competitive leagues and are specializing in a particular sport earlier than ever before. Many not only participate in one sport year round, they play and train with several different teams at a time. In some cases, athletes as young as eleven and twelve are training upwards of 27 hours a week for their sport (Caine, Roy et al. 1992). Training loads that are so heavy in duration and frequency have the potential to result in injury, particularly when the athlete in question may not be mature enough physiologically or mechanically to perform at such an intense level. One such type of injury that is associated with overuse and is unique to pre-adolescent and adolescent athletes is the physeal, or growth plate, fracture. This injury, particularly as it occurs in the proximal tibia, is the main focus of this thesis.

The physis, alternatively called the epiphyseal plate or growth plate, makes reference to the region in bones where longitudinal growth occurs. It is located between the epiphysis, the end sections of the bone, and the shaft, or diaphysis. The aggregate properties of the growth plate most closely resemble those of cartilage and fibrocartilage, gradually ossifying into bone. As in cartilage, the presence of an extracellular matrix consisting of a large amount of water endows the growth plate with vastly different material properties than the surrounding bone. In addition, studies suggest that this particular type of cartilage is less resistant to general stress than adult articular cartilage (Micheli 1986). The physis remains in this cartilaginous state until the bone is finished growing, at which point the growth plate calcifies and unites with the neighboring epiphysis and metaphysis (Martin, Burr et al. 1998). This ossification may lag behind the linear growth of the bone, which means this area of the bone is

temporarily more fragile and subject to injury.

There are several factors that render biomechanical and risk analysis of growth plate fractures different from that of other bone and overuse related injuries. One such issue arises from the fact that the pre-pubescent kinematics of movements such as running and jumping as are often different from their adult counterparts. For example, Russell et al. looked at differences in landing patterns between sexes and pre (average age 9.5) and post (average age 24) puberty. The younger group showed greater extension at both the hip and the knee, which was indicative of a stiffer landing. The children also had higher peak vertical ground reaction forces (VGRF), as well as shorter time to peak VGRF, even when accounting for body weight (Russell, Croce et al. 2007). The combination of these two factors equals less time in which to distribute and dissipate a larger impact, suggesting that these young athletes are employing different, and perhaps less favorable landing strategies than their adult counterparts. If these suboptimal movements were performed repeatedly, there would be numerous opportunities for catastrophic injury, or for accumulated minor damage.

Another suggested contributing factor to physeal fractures is that during adolescence, multiple aspects of the musculoskeletal system are in a constant state of flux. Not only are the upper and lower limbs undergoing rapid changes in mass and length, but the rate at which they are evolving can have sharp increases as well. Studies have recorded a peak height velocity of up to twelve centimeters per year in pubertal boys, with tibial length increasing an average of 10% (Bundak, Darendeliler et al. 2007), (Abbassi 1998), (Macdonald, Kontulainen et al. 2005). The problems with such quick changes in tibial length are twofold. First, an increase in diameter and/or cortical bone mass is typically subsequent to the change in length, thereby altering the inertial properties of the bone, and shear stress and bending moments experienced at the ends of the bone increase. Second, multiple studies have found that the age of peak lean body mass (LBM) velocity, an indicator of muscle strength, precedes the age of peak bone mineral content (BMC) velocity by an average of 6 months (Iuliano-Burns, Mirwald et al. 2001; Rauch, Bailey et al. 2004). This window certainly provides an opportunity for injury through increased muscle forces acting on bone that is not yet able to withstand the larger loads.

As a result, during periods of rapid growth, the muscles and tendons may be operating from an elongated resting position. This results in a tighter quadriceps-

patellar tendon unit, and hence values of pre-stress (Alter 2004). This means that areas at and near the tendon insertion point are consistently under higher levels of stress and strain than before puberty when the tibia is shorter or after puberty, when soft tissues and bone are at their adult values.

The structural and material properties of the biological tissues that compose tendon, muscle, and bone are also in transition. The ability of one area or body to sustain or apply a larger force often develops before that of the attached or surrounding tissue. The period in which the lagging entities attempt to 'catch up' presents a window in which there is an increased possibility of microscopic and macroscopic damage, fatigue, and failure. For example, Wolf's Law that states that bone will adapt and remodel to better handle the magnitudes and directions of loads it experiences. This process is certainly at work in adolescents; moderate loads and loading rates are vital to developing strong and healthy bones in young adults. However, it does take time for these changes in bone mass and geometry to respond to physiological stresses, and especially to the stress levels above this basic level experienced during extended and repeated athletic competition. A combination of suddenly higher muscle forces and/or an excessive number of cycles with little or insufficient recovery time overloads the bone before it has an opportunity to adjust. An increase in tendon collagen cross-linking throughout maturation combined with the tendon's large strength in tension translates into failure of the growth plate before that of the tendon despite the higher stresses seen in the knee.

Fifteen to twenty percent of childhood long bone fractures involve the growth plate (Wheeless 1996). The consequences, much like the etiology and mechanism of these fractures, are distinct from those encountered in adult stress fractures. They are, in fact, similar to stress fractures in that minor microscopic damage to the epiphyseal growth plate cartilage is often self-limiting with a decrease in activity or a change in sport, say from basketball to swimming. This lessens the offending loading situation, and provides the weakened bone with a period in which to heal. However, more severe fractures can result in premature closure or widening of the plate, stunted growth, and limb length discrepancies. In these cases, surgery and screw fixation of the growth plate may be necessary. These issues have the potential to impact quality of life into adulthood. Of particular concern with malalignment is an alteration of the normal stress distributions in the involved limb, increasing the probability of soft tissue

degeneration and osteoarthritis. Because of these hazards, and with levels of competition, intensive training, and sport specialization increasing at younger ages, it is important to investigate the stresses and strains that have the potential to weaken and fracture growing bones.

Clinical Relevance

Two of the major factors that are determinants for physeal injuries are the mechanical properties of the growth plate itself and the forces experienced by the physeal cartilage and the surrounding bone. In addition, knowledge of the possible locations of fracture initiation and propagation have important implications for diagnosis and treatment. Both mathematical and computer modeling can be employed to quantify how loads, stresses, and strains change from childhood to adulthood. In doing so, such models provide additional information for the prediction and care of physeal fractures in adolescents.

Problem Statement

The aims of this thesis are as follows:

1. Review and summarize the literature and current knowledge pertaining to adolescent physeal injuries.
2. Develop a two-dimensional mathematical model to examine changes in force directions and magnitudes in an isometric knee extension between children and young adults.
3. Apply the forces derived from the model in a finite element model of the tibia in order to quantify and visualize differences in location and peak values of stress in the adolescent tibia, particularly in the growth plate region.
4. Expand the results of these investigations to suggest future applications and directions in research in the areas of overuse injuries in adolescents.

CHAPTER II: LITERATURE REVIEW

2.1 Anatomy

2.1.1 Growth Plate Anatomy & Long Bone Growth

The growth plate, or physis, is a cartilaginous region close to the end of the bone, located between the epiphysis and metaphysis. It is comprised of three major zones: in order from epiphyseal to metaphyseal side they are the reserve, proliferative, and hypertrophic zones. These zones are classified according to the developmental stage of the chondrocytes as well as the organizational structure of the macromolecules. Chondrocytes are the cells also seen in articular cartilage, and are responsible for the creation and organization of the organic element of the extracellular matrix. This matrix is approximately 80% water and 20% macromolecules such as proteoglycans and collagen, which provide tissue strength and support, largely in compression.

The reserve, also called the resting zone, is attached to the epiphyseal side of the bone. This zone has the highest collagen content, and the chondrocytes and collagen are randomly scattered throughout. Little or no growth takes place here, but since the epiphyseal artery, which provides oxygen and nutrients to other zones, passes through the region, damage to this section has the potential to result in a stoppage of growth.

The proliferative zone is where the chondrocytes divide rapidly and arrange into columns. It is also responsible for most of the longitudinal growth of the bone. As they proceed distally, the cells continue to accumulate calcium, increase in volume, and prepare to mineralize in the hypertrophic zone. The area between these zones has proven to be the most susceptible to fracture, particularly at the intersection of the calcified and uncalcified cells.

In the transition from the hypertrophic zone to the metaphysis there exists a mineralization or calcification zone where the chondrocytes die and release their calcium as they progress toward the metaphysis. Near the metaphyseal junction, the cartilage matrix is broken down, and finally at the metaphysis/diaphysis junction osteoclasts resorb the spongy bone, and osteoblasts form new cortical bone. (Martin,

Burr et al. 1998), (Iannotti, Goldstein et al. 2000), (Baratz, Watson et al. 1999)). Figure 1 depicts the zones of the growth plate.

The physeal plate in the proximal tibia is responsible for approximately fifty-five to sixty percent of its longitudinal growth, so any damage to this physis has the potential to cause serious limb length discrepancies (Peterson 2007).

2.1.2 Fracture Classifications

The majority of the literature discussing physeal fractures references the Salter-Harris classification system, which identifies five types of fracture, depending on the location and path of the fracture. Table 1 and Figure 2 briefly describe and illustrate the fracture types. Types II, III, and IV, the classifications relevant to this thesis, are more commonly seen in overuse and sport-related contexts, and are produced by a combination of shear and tension. Types I and V are respectively caused by pure shear and compression, and are usually associated with a traumatic event, such as a car crash or a fall. These fractures are more common in children under the age of ten, whereas types II - IV are the ones typically encountered during adolescence (Chung 1976). Type II is a fracture that occurs along the growth plate that includes a separated piece of the metaphysis, and the location of the metaphyseal fragment depends on the direction of the applied load. The reserve and proliferative zones stay attached to the epiphysis. Fractures of type III and IV cross from the surface through the growth plate along the hypertrophic zone, with type IV advancing down through the metaphysis (Salter and Harris 1963)). These types are also most likely to require reduction or fixation, since displacement in these cases may result in growth disturbance and subsequent leg length discrepancies, especially if left untreated (Iannotti, Goldstein et al. 2000). **Figure 3** depicts an example of a type III fracture.

2.1.3 Transformations in Bone and Muscle Properties

One of the main changes under investigation is how bone geometry and bone-muscle relationships affect the forces acting on the tibia during maturation. Many studies have been done investigating how various musculoskeletal and biomechanical properties differ among children, adolescents, and adults. Kanehisa et al, (1994) compared the isokinetic strength and knee extensor cross sectional area between genders as well as between adults and children.

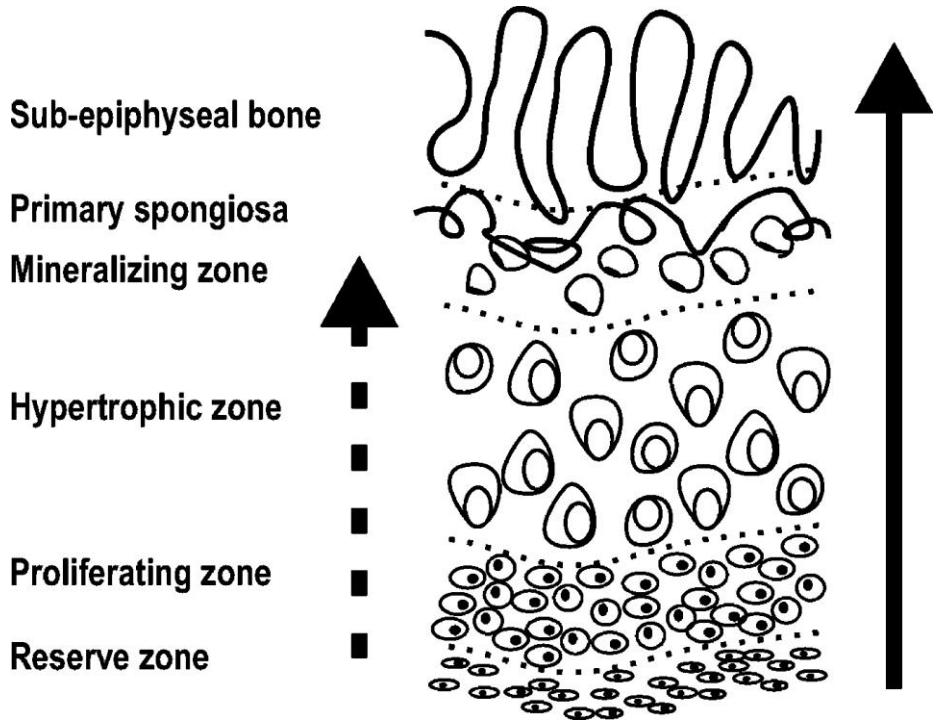

Figure 1. Depiction of Growth Plate Layers (Radhakrishnan, Lewis et al. 2004)

Table 1. Salter-Harris Classifications of Epiphyseal Fractures (Wheeless 1996)

TYPE	DESCRIPTION
I	Fracture across the growth plate separates epiphysis form metaphysis
II	Fracture divides epiphysis & metaphysis except for a chip of metaphyseal bone that is pulled w/ epiphysis
III	Fracture separates a of piece of epiphysis and a part of the growth plate from the rest of the epiphysis
IV	Fracture crosses physis, and separates a portion of the metaphysis, physis, and epiphysis
V	Severe axial loading compresses the physis traumatically

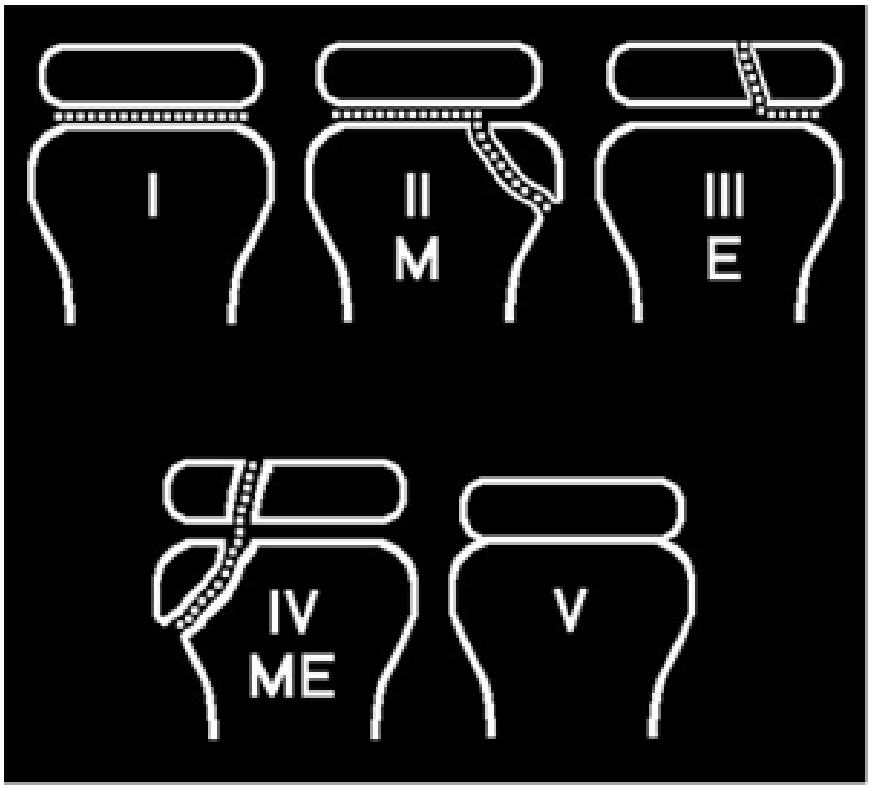

Figure 2. Salter-Harris Classifications. 'M' designates that the fracture runs through the metaphysis, and 'E' designates that it runs through the epiphysis.

Figure 3. Lateral view of a type 3 fracture with mild posterior displacement of the epiphysis and widening of the metaphysis. Subject was a fifteen year-old boy injured preparing to take off from a jump while playing basketball (Peterson 2007).

The extension tests were performed with an isokinetic dynamometer. This apparatus can provide variable opposition throughout the movement so that the velocity remains constant, while a transducer monitors the force being applied. The dynamometer is measuring torque output, so force and moment can therefore be derived from one another through the equation

$$M = F * d$$

Where *M* is the moment in Newton*meters, *F* is the force at the ankle, and *d* is the length of the lever arm – in this case, the tibia.

The age ranges for the subjects were 6 - 9 years for the children and 18 – 25 years for the young adult groups. Cross-sectional area of the quadriceps femoris was measured for each subject, as were strength at constant velocities of 1.05, 3.14, and 5.24 radians/second ($\approx$ 60, 180, and 300 degrees/sec). The investigators found that the adults had significantly higher ratios of strength to CSA multiplied by thigh length [N/(cm^2•m)], and that this difference was more pronounced at larger velocities (Kanehisa, Yata et al. 1995). This is a significant result in that it illustrates the large jump in quadriceps strength as a function of muscle mass experienced between childhood and adulthood. This increase in dynamic muscular ability occurring before the growth plate has an opportunity to ossify and strengthen accordingly would be a significant contributor to stress and strain on the proximal tibia via the quadriceps and patellar tendons.

McKay et al. (2005) investigated the ground reaction forces (GRFs) across a range of jumping-related activities. The children jumped on a force platform, and maximal GRF, maximal rates of force, and time to maximum force were measured for seventy children aged 8.3 - 11.7 years old. Among the types of jumps attempted were jumps off a box, side-to-side jumps over a barrier, and plyometric jumps, which consist of a drop-jump immediately followed by maximal effort jump. The plyometric jump produced both the largest maximal GRF (5.5 times bodyweight) and rate of change in force (514 times BW/sec) (McKay, Tsang et al. 2005). These types of movements are heavily utilized in training for sports played by populations most likely to experience proximal tibial overuse injuries: participants in basketball, soccer, and track and field.

In addition to forces acting on the limbs, it is necessary to determine how the mass and geometry of the bones change during puberty. One such study (Macdonald,

Kontulainen et al. 2006) measured total bone CSA, cortical area, average cortical thickness, muscle CSA (MCSA), section modulus (Z), and bone-muscle strength in bending, defined as

$$\frac{2 * Z}{(\text{Tibial Length}) * \text{MCSA}}$$

in one-hundred and twenty-eight adolescents. The section modulus, a measure of the ability to resist bending stress, is defined as

$$Z = I/d$$

with

$$I = \pi/4 * (R^4_O - R^4_I)$$

where *I* is the second moment of area, *d* is the distance from the neutral axis, R_o and R_i are the outer and inner radii of the bone. The subjects were separated into early, middle, and late groups based on their Tanner classifications of puberty at the beginning and end of the experiment. The largest increases in boys occurred in the last stage of puberty, with 36.8% and 28.2% increases in tibial length and muscle cross-sectional area. In girls, however, the most considerable change in tibial length was only 7 percent, and occurred in the early stages of puberty. MCSA increased by nearly equal amounts during early and mid-pubertal stage at 17.7 and 18.8 percent respectively. One of the most significant outcomes of this study was that bending bone-muscle strength as represented by both cortical area and strength index as defined above actually decreased in girls in the mid-pubertal group and boys in the late-pubertal group.

Another important study looked at work absorbed and bone deflection in addition to the bending strength and modulus through a wide range of ages (Currey 1975). This study discovered interesting trends between children, adolescent, and adult bone. Bending strength and modulus decreased between the ages of eight and fourteen before increasing again, deflection increased between ages eight and thirteen before decreasing again, and work absorbed decreased between eight and fourteen. This investigation provides evidence that supports the idea that there exists of a brief window in which there is an increased risk of fracture for the adolescent. During this period there is a decline in bone compliancy before the bone increases in strength. This is also juxtaposed with an increase in musculotendonal forces acting across the bone.

2.2 Youth Athletics and Injury

2.2.1 Case Studies

In France, six athletes, average age sixteen, were treated for tibial avulsion fractures. All five injuries for which the mechanism was known occurred on either a jump landing or takeoff. Based on experience and the cases presented, the authors suggested four methods of injury: two movements involving a flexed and two a nearly extended knee. The flexed knee injuries involved a) landing on one foot and b) preparing to spring off for a jump. The latter involves a strong eccentric contraction of the quadriceps attempting to force extension with a planted foot. Extended knee injuries result from a) jumping off with a leg nearly extended or b) landing with the involved knee undergoing a large force transmitted by a contracted quadriceps (Mirbey, Besancenot et al. 1988). This and other studies (Lian, Engebretsen et al. 2005), (Niemeyer, Weinberg et al. 2006) also identified a higher incidence of tibial physeal fractures in sports requiring bursts of speed, jumping, and quick changes in direction, such as basketball, volleyball, and track.

Niemeyer gathered data relating to nineteen adolescent athletes diagnosed with a stress fracture that came into his university hospital, with some revealing results. All but one patient played a sport that required endurance and/or sudden stops and changes in direction. The most frequently fractured site was the proximal tibia, with ten incidences. Only two of the individuals were overweight (BMI over 25 kg/m^2), hinting that increased weight is a lesser or non-factor in physeal injuries.

Another six-subject study focused on fractures that widened down into the metaphyseal portion of the bones at the knee joint (Laor, Wall et al. 2006). Half of the subjects experienced a fracture of the proximal tibia. Table 2 shows the subject age and sport participation, the length of the physeal widening, and how the fracture was treated. The tennis player also had a physeal fracture of the distal femur. In addition, the individual refused to cease activity and did not receive treatment. While the athletes who underwent treatment recovered after one to three months of immobilization of the knee, the tennis player was still experiencing persistent knee pain four years later (Figure 4). These cases are examples of the possibility of a physeal

Table 2. Proximal tibial fracture data (Laor, Wall et al. 2006).

Age	Sport	Widening Width (mm)	Therapy
12.25	Gymnastics	17	Immobilization
11.5	Tennis	19	None
8	Football	10	Immobilization

Figure 4. Eleven year-old tennis player who refused treatment or rest for bilateral physeal fractures of the proximal tibia. Note the varus alignment (*left*) six years after diagnosis. (Laor, Wall et al. 2006)

fracture forcing an athlete to take an extended period off from their sport, as well as the long-term effects of leaving a physeal fracture untreated.

In larger-scale epidemiologic study, a survey was conducted of 85 patients with lower extremity epiphyseal fractures. The pool included 60 males and 25 females with an age range of 4-17, with an average age of 12.6 years. The most common fracture sites were the distal tibial and fibula epiphyses. These accounted for 31 and 17 cases respectively, and were mostly from skiing. Fifteen were located at the proximal tibial epiphysis. According to the Salter-Harris classifications, there were 30, 25, 8, 11, and 11 type I, II, III, IV, and V fractures. Slightly more than half were treated surgically, and of the 49 patients that participated in the follow-up, there were 9 further complications, among them 3 leg length discrepancies (Krueger-Franke, Siebert et al. 1992). Similarly, the Mayo Clinic in Rochester published a review of epiphyseal fractures that were treated over a nine year span, including their Salter-Harris classifications and treatment (Burkhart 1979). In all there were twenty-eight fractures, with twenty-four in boys and three in girls. The majority of the injuries occurred between the ages of twelve and fourteen. Fracture types II (32%), III (21%), and IV (29%) were most prevalent, occurring in children playing basketball, football, and high jump/hurdles. Treatment for most fractures was a cast, however three of the type III and seven of the eight type IV fractures required surgery, and one type II fracture resulted in a varus deformity of 20°, with a leg length discrepancy of 1.6 centimeters. This underlines the ability of epiphyseal fractures to cause loss of activity and training time for those who are treated with casts, as well as more serious and long-term consequences like surgery and anatomical deformities.

2.3 Experiments

2.3.1 Failure Modes of Epiphyseal Plate Cartilage

In 1974, Robert Bright and his colleagues performed a comprehensive mechanical study of the failure of the proximal tibial epiphyses of rats twenty-five to sixty days old. Among the properties measured and calculated for the growth plates were energy absorption to failure, nominal shear stress, and maximum tensile stress in bending. The tibial growth plates showed a marked decrease in strength during

pubescence (approximately 45 days for females, 50 for males), both in shear stress at failure and maximum bending in tension. It was found that in the failed tibiae the portion of the growth plate farthest from the neutral axis under tension – in this experiment the posteromedial section – failed first. A second test was performed in which one tibia was loaded to failure, and then the contralateral tibia was loaded at a lesser stress. From this test, it was discovered that tibiae absorbing only sixty percent of the energy needed for fracture showed signs of partial failure running posterior to anterior. Similar to a beam under a bending load, smaller internal cracks were seen where one would expect larger stresses, and are expected to be the first step in the failure of the growth plate (Bright, Burstein et al. 1974).

2.3.2 Tensile Properties of Bovine Physis

John Williams et al. (2001) tested the tensile properties of bovine growth plates in the proximal tibia. Seventy lateral, central, and medial specimens of twelve to eighteen-month old bovine growth plates were loaded in tension to failure at rates of 0.0004, 0.004, and 0.04 mm/sec. Then their response was compared to five-month-old samples at the 0.004 mm/sec loading rate. Results were such that tensile strength and Young's modulus were increased with the strain rate, and both values were found to be higher on the lateral and posterior sides of the growth plate. Notably, the older bovine growth plate was 35% stronger and failed at 65% greater strain than the younger growth plate. In addition, for some basis for human comparison, the femoral capital growth plates of two cerebral palsy human cadavers were tested, and exhibited comparable values of ultimate strain (Williams, Do et al. 2001). Since individual sections of tissue were tested, the differences in material properties may be related to the type and magnitude of load experienced in-vivo, and therefore does not necessarily indicate an inherent strength in particular areas.

2.4 Computational Methods

In biomechanics, animal and cadaver studies such as those mentioned previously have proven effective at studying some of the more basic properties of biological issues, as they provide finer experiment control and require less stringent panel approval. However, when addressing topics such as movement and injuries that are markedly different in humans, animal studies become less directly applicable. For

determining in-vivo forces and torques, telemetry has been used to successfully obtain loading values in the human hip and knee joints (Heller, Bergmann et al. 2001; D'Lima, Patil et al. 2006). Telemetric implants use force transducers and wireless and radio technology to transmit and acquire the implant data and remotely track contact forces and contact areas in the relevant joint. However, due to their invasive nature and the fact that they are typically integrated with hip and knee replacements, they are not likely to see widespread use any time in the near future, particularly in younger populations and especially in children.

2.4.1 Mathematical Modeling

An alternative to telemetry that has been employed to attempt to determine joint loading and torques is mathematical modeling. Mathematical modeling makes use of measureable quantities such as ground reaction forces, linear and angular velocities from gait analysis, in combination with contact and geometry data derived from imaging techniques such as CT and fluoroscopy to solve for unknowns. However, there are often a large number of muscular, external, and contact forces acting on a single joint or body. Mathematical models can generally be categorized by which of two approaches are employed to solve a dynamic biomechanics problem.

One such approach is an optimization method, which attempts to directly solve for chosen aspects of an indeterminate system. This technique formulates and attempts to solve ordinary differential equations based on constraints and minimization/maximization principles. Examples include a minimization of energy expenditure or a geometrical constraint. Blankevoort and Huiskes (1996) calculated knee ligament strains in extension by minimizing the differences in flexion between the model they developed and a reference set of knees (Blankevoort and Huiskes 1996). Hefzy and Abdel-Rahman (1993) developed a 2D dynamic model for the analysis of impact response by defining the tibial and femoral profiles in terms of polynomial equations and assuming that a single point between them was in contact throughout the analysis (Abdel-Rahman and Hefzy 1993). Anderson and Pandy (2001) calculated muscle forces and limb motion during walking by minimizing energy expenditure per distance (Anderson and Pandy 2001). There are two problems associated with this method. One is that the body does not always conform to minimization/maximization optimization protocols, particularly in cases when it is in an injured state. The other is

that while this method may produce a mathematically viable solution, it may not make sense physiologically.

The other method is that of reduction, which attempts to minimize the number of unknowns such that they are equal to the number of equations, resulting in a determinate system. This is achieved by making various assumptions, for example that some muscle groups are acting together (e.g. the various muscles of the quadriceps), or that certain muscle forces do not make significant contributions to the activity being modeled. This method also seeks to reduce the number of unknowns by incorporating force data from force plates, kinematic data from gait analyses, and geometric and contact data from x-rays, fluoroscopy, CT and MRI scans. Komistek et al. (1997) utilized a combination of force plate data, cadaver specimens, kinematic gait data, and fluoroscopy to develop a model of the joint reaction forces at the knee and hip during walking (Komistek, Stiehl et al. 1997). As evidenced by this particular model, which predicted joint reaction forces of 1.9 to 2.6 times body weight in the hip, and 1.7 to 2.3 times body weight in the knee, the reduction method has been more likely to produce accurate descriptions of joint forces and moments in biomechanical systems. The addition of Kane's method of dynamics, discussed in chapter III, makes the reduction method of modeling an even more attractive option.

2.5 Finite Element Analysis

Finite element analysis (FEA) is a valuable tool that allows for quick and inexpensive simulation and manipulation of anatomical, material, and dynamic parameters. Finite element method breaks down a complex two or three-dimensional geometric figure into an assembly of simpler subdivisions (finite elements) that can be assigned specific material and mechanical behaviors. These subdivisions are connected at junctions called nodes, where estimates of field variables such as stress and displacement can be assigned approximating functions. Boundary conditions such as loading parameters and movement constraints can also be applied to sections of

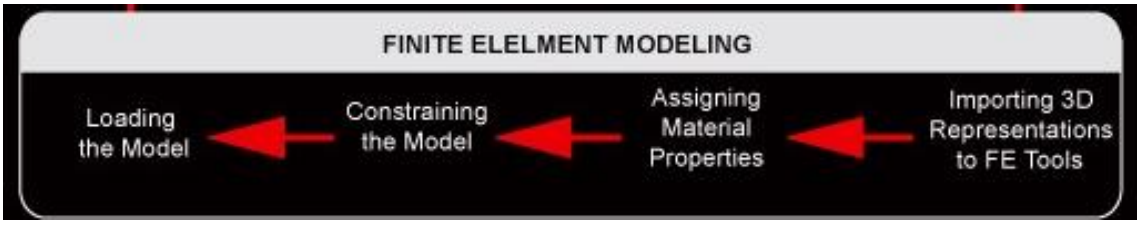

Figure 5. Finite element modeling flowchart (www.biomesh.org).

the structure instantaneously or over a specified time interval, and resulting field variables can then be computed for each individual element by solving equilibrium equations. The result is a more spatially detailed analysis that allows for visualization of behavior of interest for the whole structure as opposed to a point or a small segment. This approach is useful for detecting weak and vulnerable sections of an assembly, including its internal sections**.**

One area of biomechanics where finite element analysis is seeing increased use is in implant testing. Assessing stress, contact, and wear of implants theoretically and computationally can identify potential problems and design flaws before money is spent on large-scale manufacturing or before they are tested in vivo. In addition to implant testing, finite element analysis also has promise in other areas of orthopedics and in investigating injury risk and mechanisms. An advantage of FEA in addition to the detail of results is that it allows for investigation of single or multiple effects chosen by the researcher. For example, the effect of removing a particular muscle force or changing the size or material properties of a region or body can be isolated and computed, something that is nearly impossible or incredibly time consuming to achieve in in-vivo experiments. The main limitation of FEA, particularly in this case, is that the mesh refinement was somewhat limited by the use of a student package, limiting the number of nodes. Two particular finite element analyses have sought to investigate injuries relating to physeal fractures in youth and adolescents – one at the spine, and one at the proximal femur.

2.5.1 Slipped Capital Femoral Epiphysis

A study by Gomez-Benito et al. (2007) attempted to apply a pre-existing theoretical damage model in conjunction with a finite element model to assess the risk of a child developing a slipped growth plate at the femur-hip interface (known as slipped capital femoral epiphysis, abbreviated SCFE). The early stages of this type of injury are difficult to identify, and the longer it takes to identify the problem, the greater the severity of the slip, and the higher the possibility of complications and bone degeneration. Based on prior research, and knowledge of the strength properties of bone under different types of loading, the damage model assumed that failure was induced by a combination of shear and tension. The finite element model was based

on a fourteen-year-old patient who had a slipped femoral epiphysis in one leg, and a 'normal' contralateral leg. They utilized the models of the healthy and diseased leg and applied the damage model to generate ultimate stress and failure curves from geometric parameters such as growth plate area, neck length, and physeal sloping angle. The researchers found a strong relation between growth plate failure and body weight, and that the damage model was useful in evaluating the risk of developing SCFE (Gómez-Benito, Moreo et al. 2007).

2.5.2 Pediatric Lumbar Spine

Another FEA study conducted in Japan (Sairyo et al, 2006) was focused on the mechanical reasons behind spinal physeal fractures in pediatric patients. An adult spine model was scaled to represent the spine of the average fourteen-year-old, and its geometry and material properties were estimated from the literature. In the Abaqus™ software package, a 351 N preload and 10 N m moment were applied to the model. Von Mises stress, as well as stresses in the vertical direction were determined to be the main results of interest. The stress distribution outputs supported the researchers' hypothesis that the posterior aspects experienced higher stresses in extension than flexion, and that the apophyseal ring and growth plate in the adolescent model experienced much higher stresses than other sections of the spine. These increased stresses combined with the inherent weakness of the growth plate, much like in the tibia, can lead to injury, fracture, and disorder of growing bones (Sairyo, Goel et al. 2006).

CHAPTER III: MATHEMATICAL MODELING AND INVERSE DYNAMICS

3.1 Introduction

There are two primary forces of interest in calculating stress and strain on the proximal tibia. One is the tensile force exerted by the quadriceps, transmitted through the quadriceps tendon, patella, to the insertion of the patellar ligament into the tibial tubercle. The second is a combination of shear and compression from tibiofemoral contact forces. These forces are not directly measurable in vivo, since the only current use of telemetry in children or adolescents is in cochlear implants, and telemetric knee implants have typically been only used to measure compressive forces and contact areas. Therefore, it is necessary to turn to other methods to obtain internal muscle and joint-reaction forces at the tibia.

Dynamic mathematical models are often used for such calculations, and make use of the Newton-Euler equations

$$\sum F = m * a \quad \text{(Force = mass x acceleration)}$$

$$\sum M = I * \alpha \quad \text{(Moment = Mass moment of inertia x angular acceleration)}$$

Forward dynamics solves for the motions of the system, while inverse dynamics solves for the forces that create movement. To calculate these values at the knee joint, combinations of measurable aspects such as kinematics (e.g. acceleration and velocity from gait analysis), inertial properties (e.g. limb mass and length), and kinetics (e.g. force plate data) are used. As is sometimes the case, certain assumptions may need to be made, either for the sake of simplicity or lack of data. Some of the more common assumptions in biomechanical dynamic models include:

1. Frictionless joints
2. Segments as rigid bodies
3. Body masses concentrated at their mass centers
4. There is no co-contraction of agonist and antagonist muscles

While the first three assumptions are more often than not useful and greatly simplifying approximations, whether assumption number four is made depends on its relevance to the movement and system being modeled, as well as the unknowns the model is attempting to obtain. One way in which to simplify the model and to make this

assumption more applicable is to derive the necessary forces through analysis of an isokinetic knee extension or flexion movement (Nisell, Ericson et al. 1989; Kellis 2001). EMG tests have suggested that the hamstrings are not sufficiently activated during an isokinetic extension. Therefore, as opposed to analysis of a flexion movement, where it would be necessary to include a hamstring force, modeling an extension allows for assumption number four to be made (Osternig, Hamill et al. 1984).

The analysis method utilized here is known as Kane's dynamics, as developed by TR Kane and DA Levin (1983). Through a combination of principles based in Newton-Euler, Lagrange, and D'Alembert mechanics and dynamics, kinematics or forces of biomechanical systems can be determined through a forward or inverse analysis, respectively. Kane's dynamics employs both generalized angular velocities that characterize how a body rotates when acted on by a moment, and translational velocities that show how they move linearly with respect to an applied force. These velocities are then continually differentiated for partial velocities, partial angular velocities, and motion equations. The resulting motion equations can be solved for generalized forces that include contact, restraint, muscle, (all characterized as active forces) and inertial forces (F^*). This results in the standard equation of Kane's dynamics

$$F_r + F_r^* = 0$$

For r = 1,2,..n, where n is the degrees of freedom of the system.

One advantage of this method is a reduction of order. The Newtonian formulation of the lower leg system can yield second order equations involving acceleration (d^2x/dt^2). Using generalized speeds (u_i), the highest order the Kane method produces is first order (du_i/dt). This greatly simplifies computations and reduces the complexity of resulting equations and solutions, particularly when moving from two to three dimensions, and from single to multiple body analyses. Calculations and equations that would typically take up multiple pages may only take several lines or a few pages with Kane's method of dynamics.

3.2 Leg Extension Model

A basic 2-dimensional, sagittal-plane mathematical model of a leg extension was developed to provide a measure of the change in relevant forces at the proximal

tibia for use in the finite element model discussed in chapter five. The model also serves to provide an introductory example as to how Autolev™ (OnLine Dynamics, Inc, Sunnyvale, CA), facilitates the ease of dynamic analyses, as well as how changing individual aspects of the model can be quantified and visualized.

In this instance, mathematical and software modeling are useful in that the effect of changing a specific value or set of values can be easily investigated. Aspects of particular importance are patellar tendon force and length, contact force, height (and therefore tibial length), body weight, and speed. The effects of these variables are difficult to isolate, but might be of interest both within and across age groups. Male values were chosen for all of the analyses since boys experience physeal fractures in greater numbers, and grow more in an absolute sense and at a faster rate than girls during puberty (Alexander 1976).

The model and codes for the analysis of the knee extension were developed in the Autolev software package, a symbolic manipulator for dynamics and engineering. Autolev allows for the generation of equations of motion into Matlab™ (The MathWorks, Inc. Natick, MA), Fortran, or C codes, facilitating the creation of graphs and tables. Finally, the ANIMAKE™ program can be used to visualize the motion of the system to ensure that the motions produced are correct, which is even more useful in forward dynamics problems. The files associated with Autolev are as follows:

- __**.al** The main user-created code associated with the Autolev program.
- __**.all** Text file created by Autolev that records the calculations performed and the resulting equations.
- __**.dir** Used by ANIMAKE to visualize the kinematics of the model.
- __**.for** Fortran code
- __**.m** Matlab code
- __***.i*** Where *i* = 1,2,3… Text file containing tabular numerical data for output variables

The Fortran and Matlab codes take input values and equations, and generate the **.1**,**.2**, **.3**,… files containing tabular data.

Three reference frames are used to define the system: 1) The Newtonian, or inertial reference frame N, on the femur, 2) a body frame A, attached to the shank, and 3) a frame B associated with the patellar ligament. The $\vec{A}_1$ direction corresponds to the

proximal-distal tibial axis, the $\vec{N}_2$ is parallel to the axis of the femur, and the $\dot{B}_2$ coincides with the patellar ligament. Motion is occurring exclusively in one plane – a rotation about the $\vec{N}_3, \vec{A}_3$, and $\vec{B}_3$ directions. Therefore, the analysis becomes one of general plane motion with one degree of freedom. The flexion moment is considered positive in the counterclockwise direction. The angular velocity of the tibia in the reference frame can be defined as ${}^N\vec{\omega}^A = \dot{\theta}_1 \vec{N}_3$, where $\dot{\theta}_1$ is the rate of change of the angle between the long axis of the tibia and the $\vec{N}_2$. The transformation matrix between the tibia and the fixed Newtonian is derived as

$$\begin{Bmatrix} A_1 \\ A_2 \\ A_3 \end{Bmatrix} = \begin{bmatrix} C\theta_1 & S\theta_1 & 0 \\ -S\theta_1 & C\theta_1 & 0 \\ 0 & 0 & 1 \end{bmatrix} \begin{Bmatrix} N_1 \\ N_2 \\ N_3 \end{Bmatrix}$$

In addition, the patellar ligament frame {B} undergoes a positive rotation about the tibia frame, θ_2, and by extension can be related to the Newtonian through the equation

$$\begin{Bmatrix} B_1 \\ B_2 \\ B_3 \end{Bmatrix} = \begin{bmatrix} C\theta_2 & S\theta_2 & 0 \\ -S\theta_2 & C\theta_2 & 0 \\ 0 & 0 & 1 \end{bmatrix} \begin{bmatrix} C\theta_1 & S\theta_1 & 0 \\ -S\theta_1 & C\theta_1 & 0 \\ 0 & 0 & 1 \end{bmatrix} \begin{Bmatrix} N_1 \\ N_2 \\ N_3 \end{Bmatrix}$$

Since the segment length and mass distributions vary more with age in children between 4 and 14 (Jensen 1989), slightly different codes were written to differentiate between youth in that age range and adults.

Autolev codes were written in order to make two groups of comparisons. One was to contrast age-related changes of proximal tibial forces; the other was for the purpose of comparing forces by altering a single anatomic factor hypothesized to increase the risk of tibial fracture. Codes were written for the following:

1) An adult
2) An eight-year-old child
3) A thirteen-year-old
   a) In the 50th percentile of height and weight and with a fifty percent increase in dynamometer force.
   b) In the 90th percentile weight
   c) In the 90th percentile height

d) With a patellar tendon length ¾ that of the baseline adolescent model

e) With a seventy-fifth percent increase in dynamometer force

The 50th percentile height and weight adolescent values were used for the age comparison, and as the baseline value for factor analysis. Percentile height and weight values were obtained from United States census data via the Center for Disease Control (2000). The equations used to calculate center of mass and segment length are in Table 3. The inputs for dynamometer force, body weight, and height for the adult and child codes were the averages determined in the previously mentioned study by Kanehisa, and are shown in Table 4. The adult Autolev and Fortran codes, as well as the adolescent output Autolev and Matlab™ codes, are presented in the appendix.

Table 3. Body segment parameters (Jensen 1989).

	L (%BH)	**Mass (%BW)**	**%L_{CoM} (from distal)**
Children <14y	23.3	0.122*age+3.809	55.74+0.3*age
Adults	23.3	4.6	57

Table 4. Average values used for youth and adult Autolev models. The force is the dynamometer force at the ankle, at the various constant speeds (Kanehisa, Yata et al. 1995).

	Age (y)	**Mass (kg)**	**Height (m)**
Youth	8	24	1.229
Adult	36	62	1.701
	1.05 rad/sec	**3.14**	**5.24**
Force (N)			
Boys	141.1	95.4	58.7
Men	472.1	336.3	220.5

Table 5. Property values for the factor comparison Autolev codes. Models were defined by which aspect was changed from the baseline model.

	Height (m)	Mass (kg)	Force (N)	Patellar Ligament Length (cm)
Model				
Baseline	1.56	46	250	2.94, 2.29, 13.7
Patellar Ligament				2.205, 1.72, 10
Force			325	
Weight		60		
Height	1.75			

Figure 6, Figure 7, and Figure 8 depict the femorotibial and tibia/patellar tendon coordinate systems and points.

Verification that the point, body, and movement definitions were correct was achieved by running the animation file in the ANIMAKE software (Figure 9).

3.3 Results

3.3.1 Age Comparison

As anticipated, the patellar tendon and contact forces increase a great deal from the youth to the adult models. Maximum patellar tendon force, femorotibial shear, and normal contact forces all increase approximately three and a half times. The main aspect of concern from these results is the patellar tendon force. For one, the changes in shear force are much smaller in magnitude. With regard to the normal forces, the bone is less likely to be fractured in compression than in shear or tension. In addition, the mechanism of most overuse physeal injuries is the result of shear, tensile forces, or a combination of the two.

Although the absolute force levels decrease as the extension speed increases from 60 to 180 degrees/second, the percent increase of maximal force acting at the patellar tendon insertion increases nearly two hundred and fifty percent from the youth to adult values. The force levels increase slightly again as the speed increases from 180 to 300 degrees per second. This increase in muscle capacity may precede and actually stimulate the adsorption of stronger bone normally.

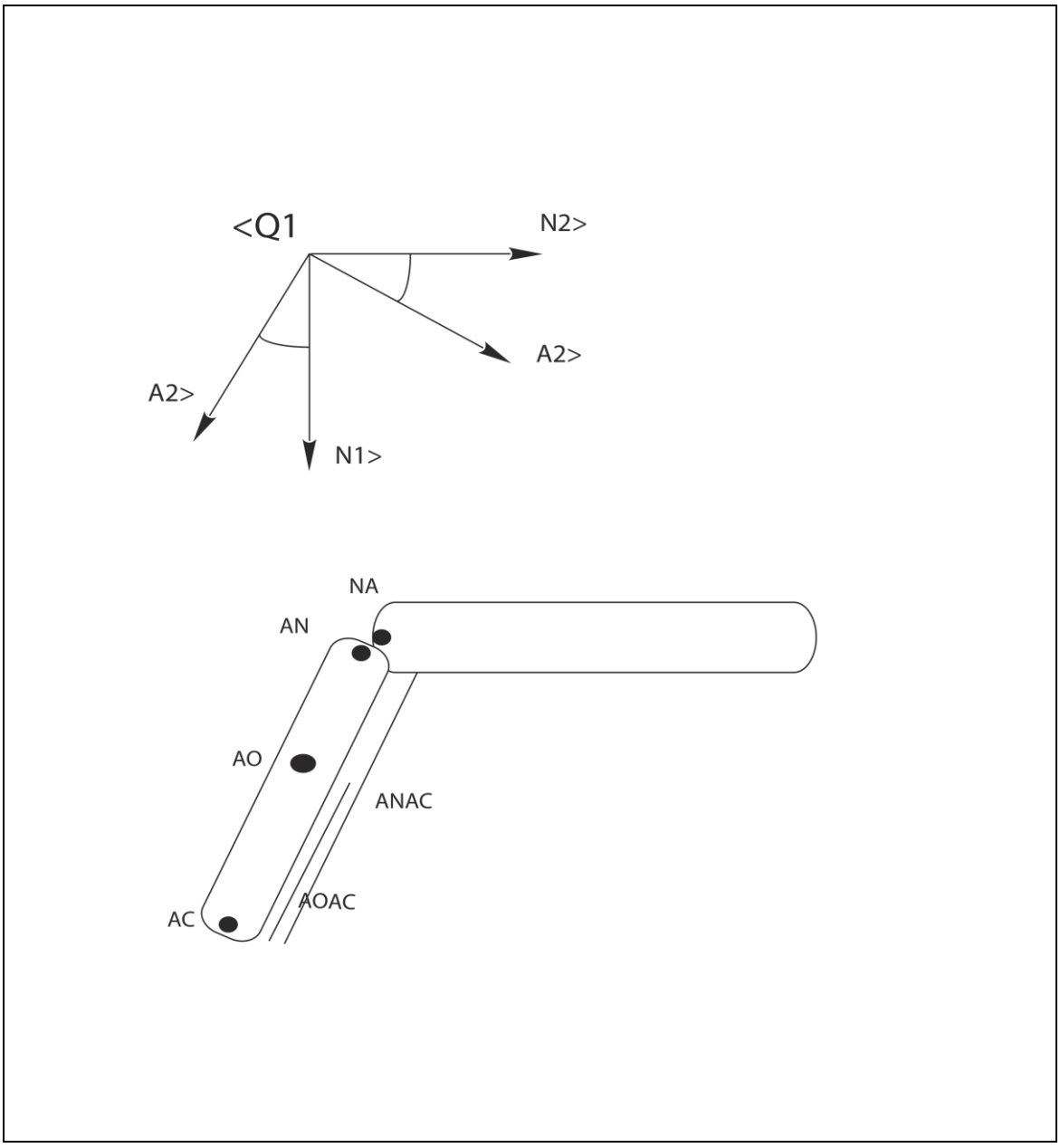

Figure 6. Femorotibial points and frames. NA - contact point on the femur, AN - contact point on the tibia, AC – distal end of the tibia, AO – center of mass of the tibia, ANAC – length of the tibia, AOAC – distance from the CoM to the distal end of the tibia.

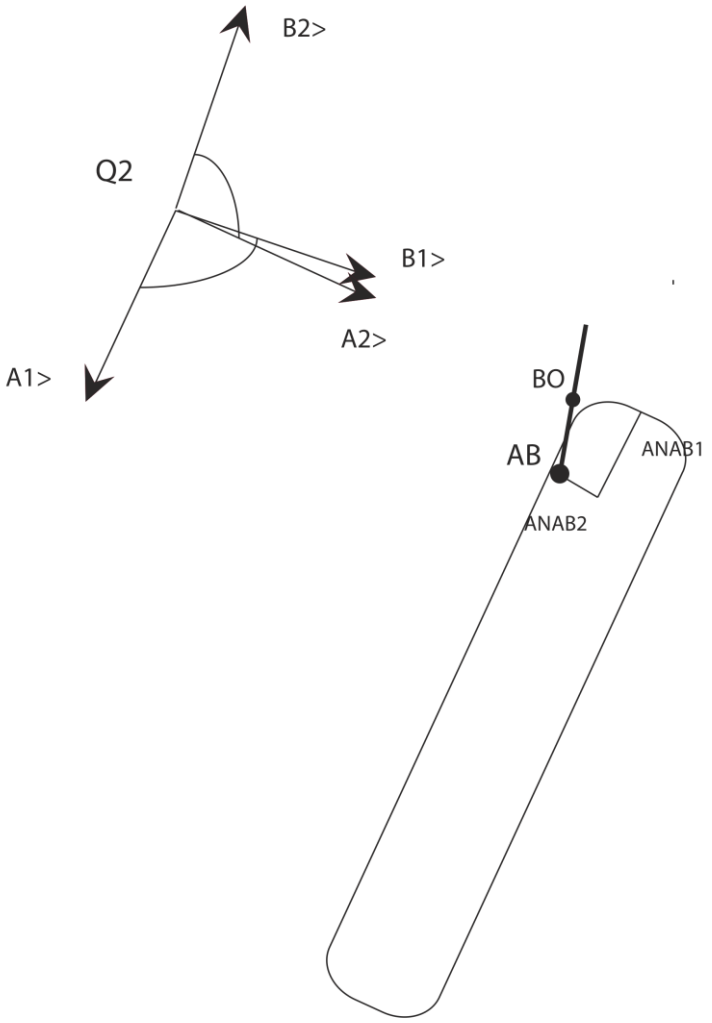

Figure 7. Patellar Tendon/Tibial points and frames. AB – Patellar tendon insertion point, BO – midway point of patellar ligament, ANAB1, ANAB2 – distance from the proximal end of the tibia to the patellar ligament insertion point in the A1> and A2> directions.

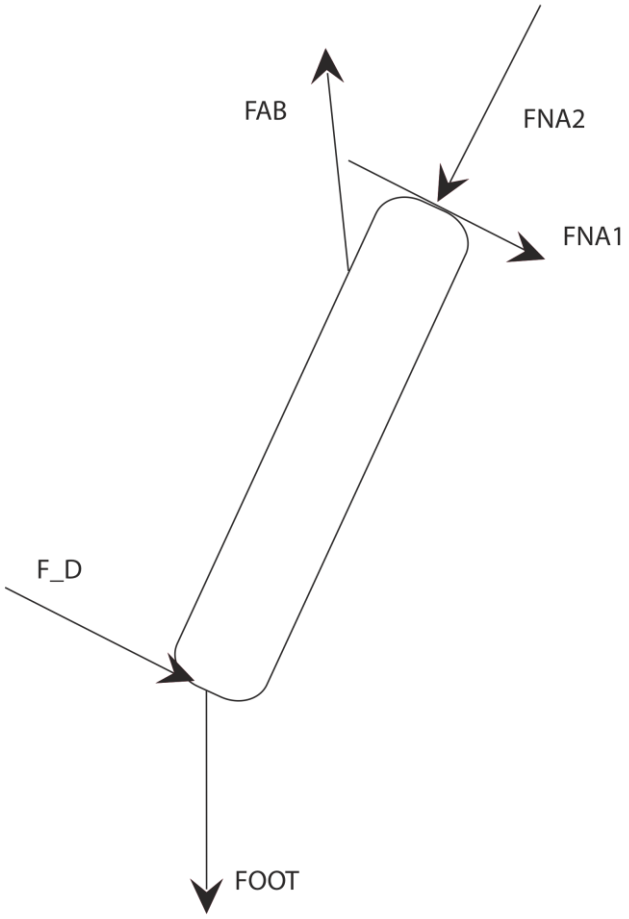

Figure 8. Forces acting on the tibia during an isometric leg extension. FNA1, FNA2 – femorotibial shear and normal forces, FAB – patellar ligament tensile force, F_D – dynamometer force acting at the distal end of the tibia, FOOT – weight of the foot.

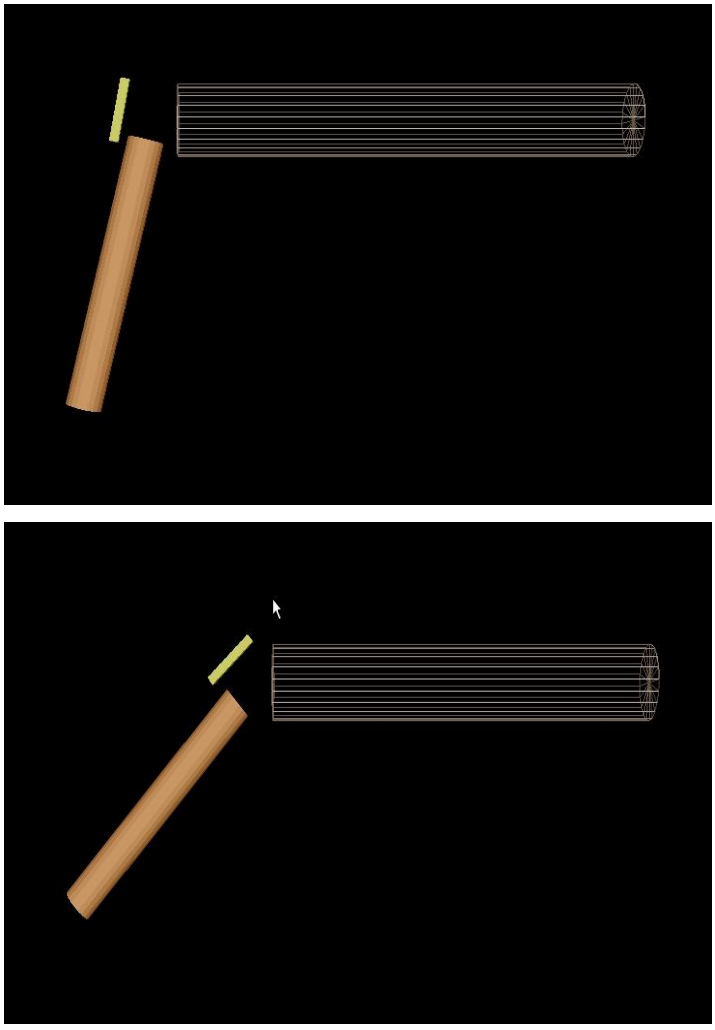

Figure 9. Animation snapshots of adult Autolev code at t = .10 and t = .75 seconds.

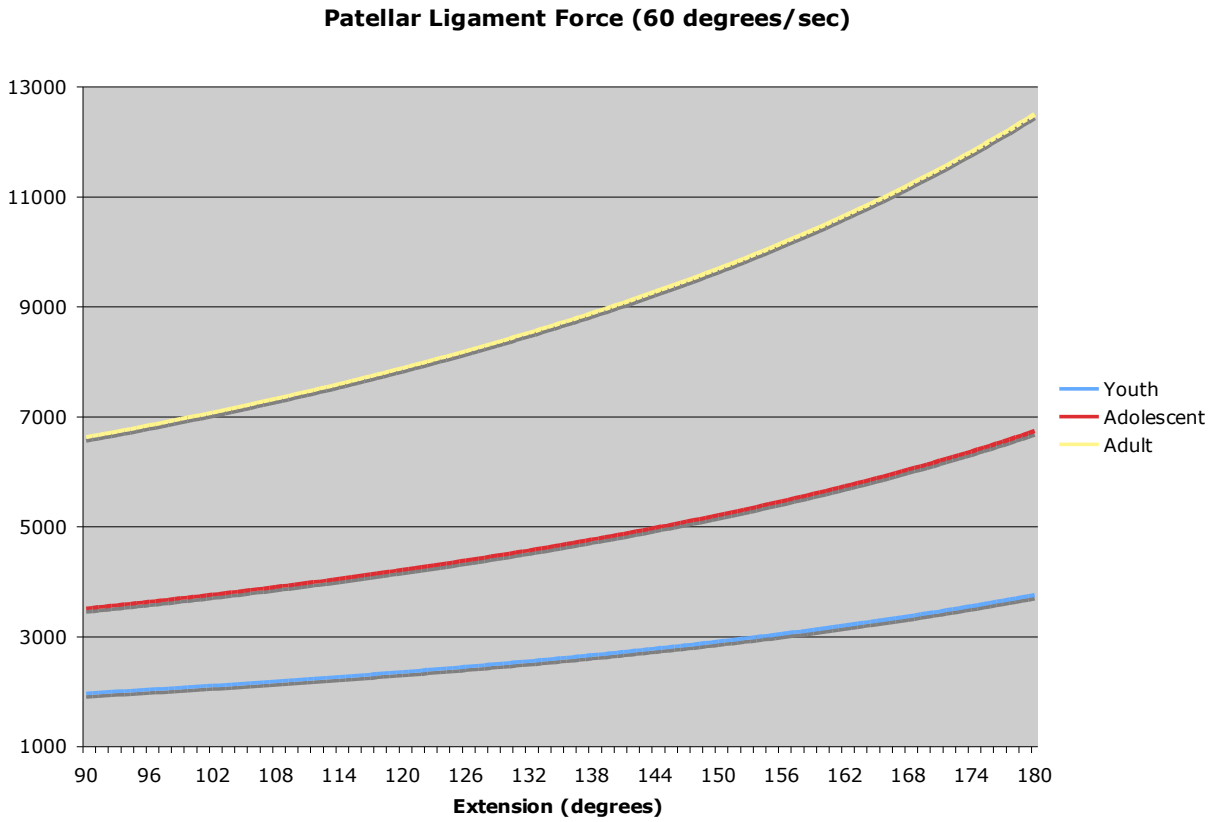

Figure 10. Age related change in patellar ligament force at 1.05 radians per second.

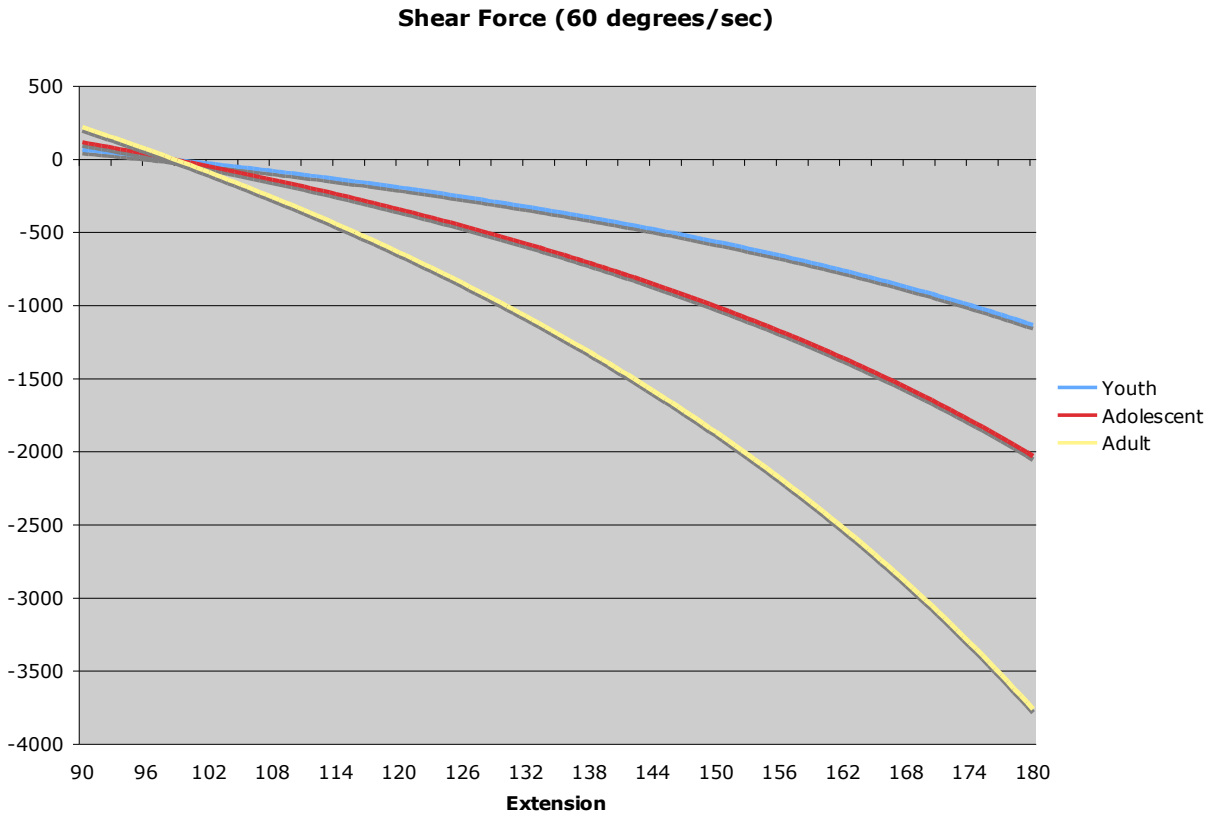

Figure 11. Age related changes in tibiofemoral shear force at 1.05 radians per second

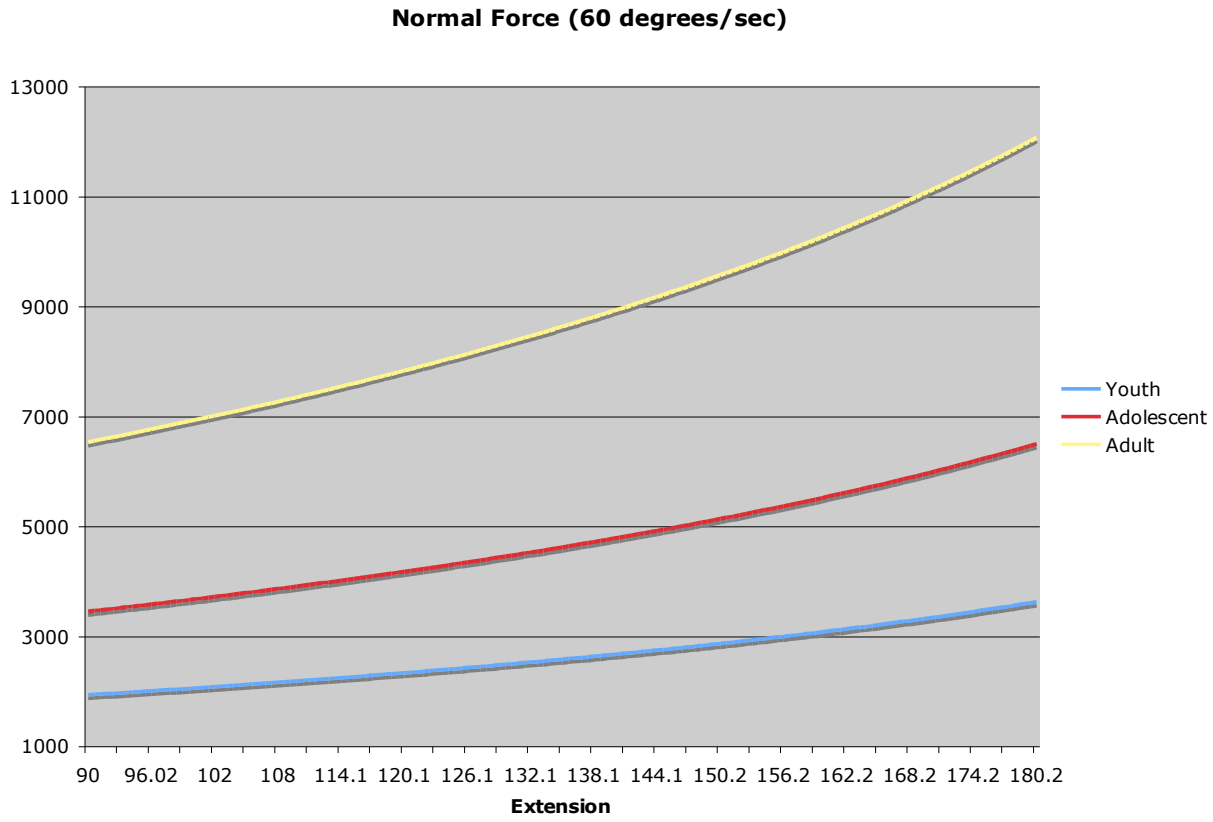

Figure 12. Age related changes in femorotibial normal force at 1.05 radians per second.

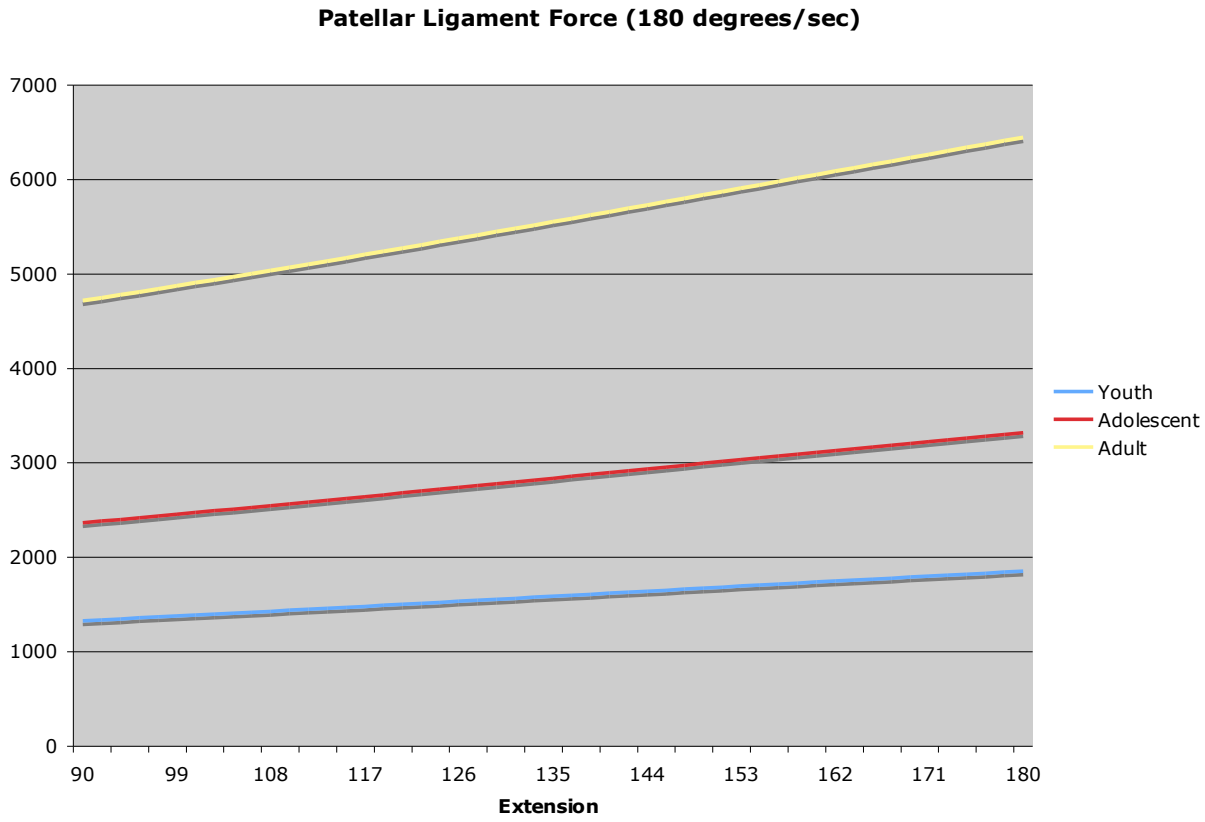

Figure 13. Age related change in patellar ligament force at 3.14 radians per second. Body weight normalized forces can be found in Appendix A.

Therefore, while physiologic and moderately high levels of activity are positive and even necessary for adequate bone development, exertion to far above a certain level would cause microdamage to the bone, with numerous cycles leading to fracture. As a result, parents and coaches should be wary of encouraging young athletes to increase their muscle mass beyond what they would accumulate naturally through large amounts of weight lifting and/or increased protein intake, at least before or during the ages at which they are growing at their peak velocity.

3.3.2 Individual Factor Comparison

The individual factor comparison results provide some clarification as to which aspects of growth play a larger role in the overloading of the physeal region. The increased dynamometer force and shortened patellar ligament models produced similar magnitudes and resulted in the most significant increases for both femorotibial contact and patellar ligament forces. The largest changes in loading occurred at the patellar tendon insertion – increasing by thirty-three and seventy-eight percent for slow and medium speeds. The shortened patellar tendon and dynamometer force relate to two issues. One is the increase in muscular force discussed in the age portion of the results. The other is the idea that the force at the proximal tibia is increased by a patellar ligament acting from a shortened length, and is therefore “tight’, and likely acting at an increased preload. This results in a smaller range of movement before the ligament reaches the limit of its slack and the tibia experiences a greater tensile force for a greater portion of time. If this is a root cause, this particular issue may be abated through adequate stretching programs, particularly before bouts of physical activity.

It is also important to realize that though differences may be slight or moderate, these differences can accumulate quickly when performing a movement with frequency. For example, an athlete may execute a soccer kick dozens of times a practice session, four or five times a week. These types of force estimations can be useful in risk analysis, using a load/cycles to failure model.

Changes in weight contribute the least to the forces at the proximal tibia. This idea of weight as a minor factor is consistent with conclusions drawn in discussion of the Niemeyer case study, yet divergent from the findings of the Gomez-Benito finite element analysis of the spine, emphasizing that causes of failure in different bones and

even at proximal versus distal ends of the same bone may be different, and as such need to be studied in detail separately.

One last result to note, however, is that at increased speeds, the calculated maximum patellar tendon force is still forty-seven percent higher in the 90th percentile weight model than the baseline. The effect of the forces on the tibia in conjunction with the weaker material of the growth plate is the subject of the finite element analysis in chapter IV.

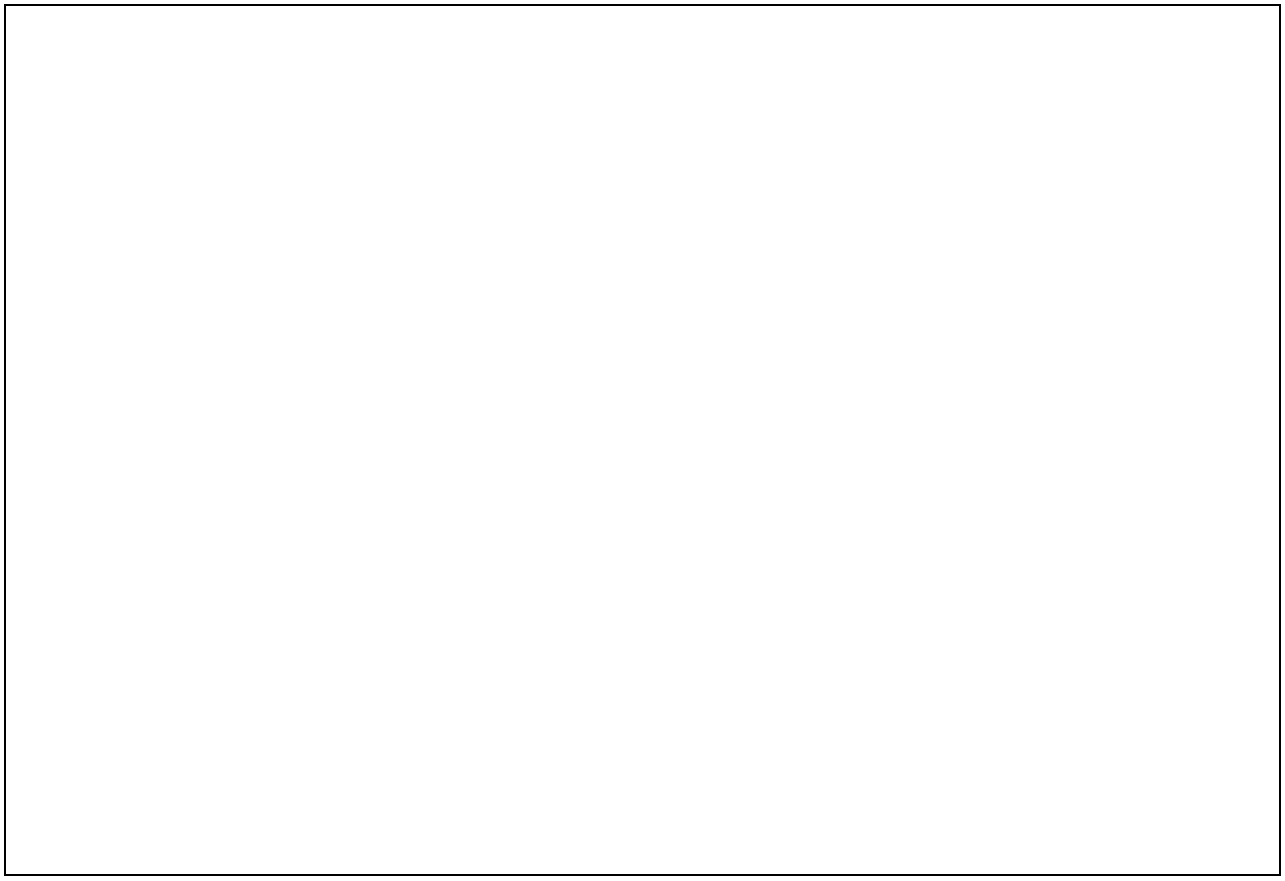

Figure 14. Factor related change in patellar ligament force at 1.05 radians per second.

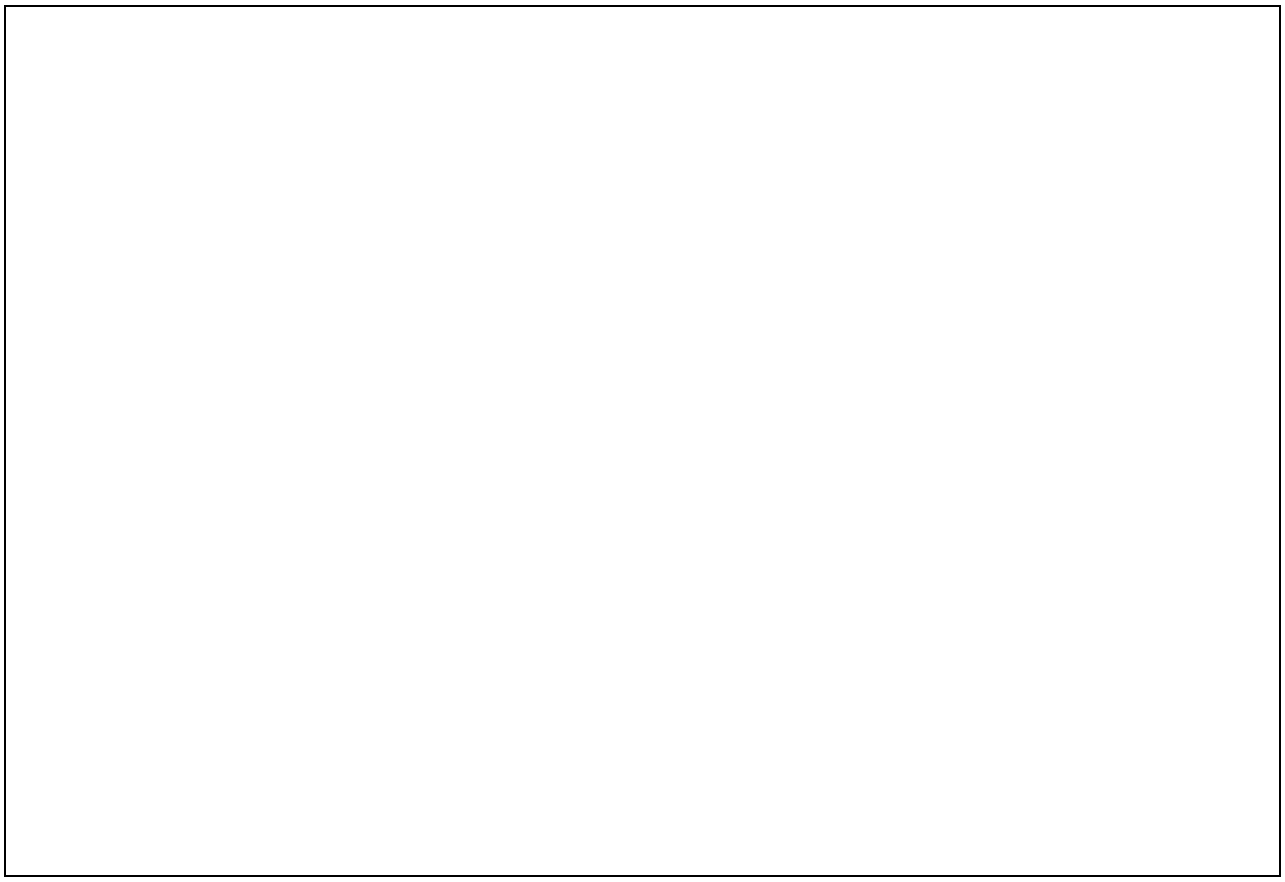

Figure 15. Factor related change in patellar ligament force at 3.14 radians per second.

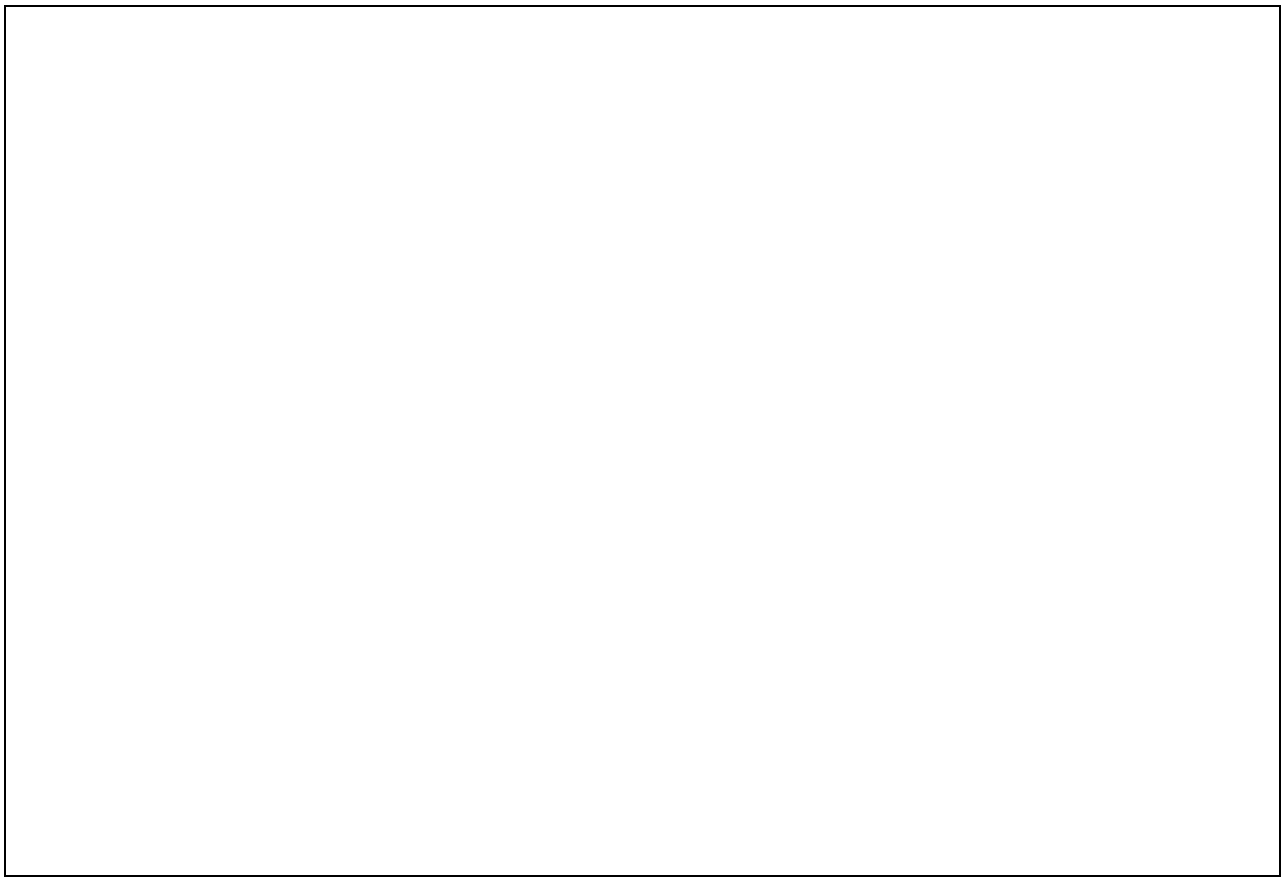

Figure 16. Factor related changes in tibial shear force at 1.05 radians per second.

Figure 17. Factor related change in femorotibial normal force at 1.05 radians per second.

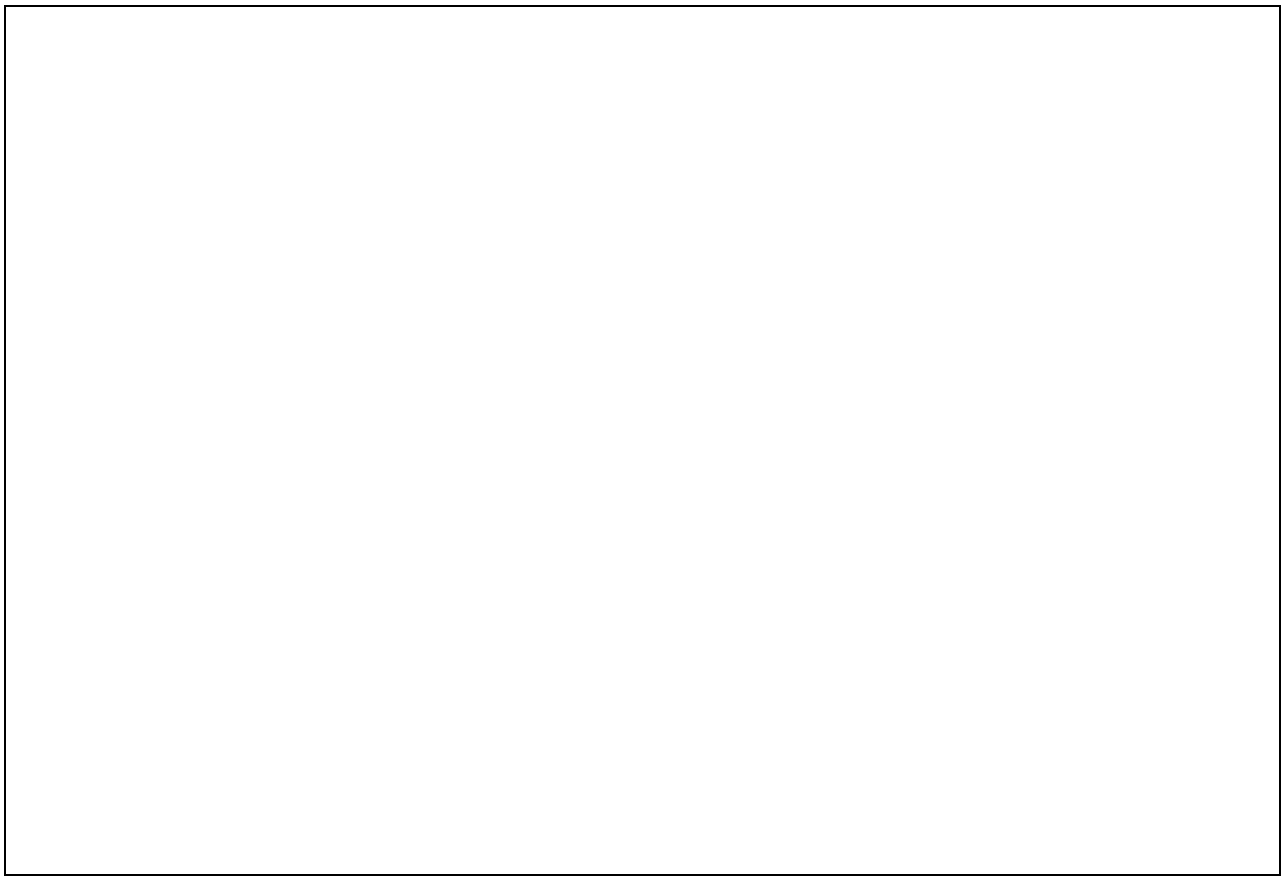

Figure 18. Factor related change in femorotibial normal force at 3.14 radians per second.

CHAPTER IV: FINITE ELEMENT ANALYSIS

Although the load type is related to the mode of fracture, it is important to recognize that the loads produced in the bone are often the net result of several external shear, compressive, tensile, bending, and torsion forces. In addition, these same combinations of forces may produce varied effects on tibiae composed of differing material properties. Incorporating forces and qualities into a three-dimensional model can provide clues as to how loads induce the stresses that contribute to particular fracture patterns.

4.1 Assumptions

1. Negligible friction
2. Rigid bodies
3. Transversely isotropic materials
4. Uniform growth plate thickness

A main source of friction in the knee joint is seen more often in older individuals who have experienced wear in the joint's articular cartilage. Since this investigation centers on a comparison between children, adolescents, and young adults with relatively new and healthy joints, bone-on-bone friction in particular is not a concern. The rigid body assumption has also been tested; Halloran et. al investigated the variability introduced by both element mesh size and rigid verses deformable body analyses in total knee replacement force and contact. The conclusions were that when performing an explicit finite element analysis, a finer mesh delivered slightly more accurate results (to a non-significant level), and the rigid body assumption yielded nearly identical results, while reducing computational time from eight hours to as little as eight minutes (Halloran, Petrella et al. 2005).

Bone is not linearly isotropic, and the growth plate, similar to articular cartilage, exhibits biphasic and viscoelastic behavior. Unfortunately, at present, studies done to test the stress response of the growth plate have focused on compression. In similar FEA studies (Sairyo, Goel et al. 2006; Sairyo, Goel et al. 2006; Gómez-Benito, Moreo et al. 2007) linearly isotropic properties for both cortical and cancellous bone were also

assumed, and produced useful results. For the purposes of this analysis, it was deemed that the accuracy of results would be improved by modeling both cortical and cancellous bone as transversely isotropic, with the axis of symmetry along the length of the tibia. Although there is some fluctuation in the thickness of the growth plate depending on location, the variability is on the order of hundredths to tenths of a millimeter (Williams, Do et al. 2001).

4.2 Model Description

The finite element model used in the following simulations was based on a tibial part contributed to the open source model database (Ardatov 2006). The basic geometry was imported into the FE software package Abaqus™ (HKS, Pawtucket, RI), and the part was partitioned in order to refine the mesh size as well as to delineate sections for different material properties. The tibia was 35 centimeters long, translating to a height of approximately five feet (based on the Jensen equation previously mentioned), consistent with a typical pre or early adolescent height. The tibial tray was eight centimeters mediolaterally, and six centimeters anteroposteriorly.

4.2.1 Material Properties

Three materials were defined and assigned to sections of the adolescent model: cortical bone, cancellous bone, and growth plate cartilage. Values for the Young's Modulus, Poisson's ratio, shear modulus were determined from a literature survey of mechanical testing and computational studies attempting to describe the properties of bone and cartilage (Yoon, Yang et al. 2002), (Hoffmeister, Smith et al. 2000), (Ford and Keaveny 1996), (Sairyo, Goel et al. 2006).

In order to isolate the effect of the bone strength, three of the four models were identical in size and applied load. The main model was designated with lower range constants, and an approximately eight millimeter growth plate partition between two areas of cancellous bone at the proximal end of the tibia. This model is designated as the 'weaker' or 'adolescent' model, and is the subject of comparison to the subsequent models discussed. A second model was given upper range strength constants, and was assumed to consist entirely of cortical and cancellous bone.

Table 6. Young's and shear moduli used in Abaqus simulation. Values are in MPa.

Model 1				**Model 2**		
(Adolescent)	*Cortical Bone*	*Trabecular Bone*			*Cortical Bone*	*Trabecular Bone*
E_1	9000	600		E_1	14000	800
E_2	9000	600		E_2	14000	800
E_3	14000	2000		E_3	20000	3000
G_{12}	3500	200		G_{12}	6500	300
G_{13}	5000	300		G_{13}	8000	400
G_{23}	5000	300		G_{23}	8000	400

To investigate the any potential effects of the possible viscoelastic nature of the growth plate, one adolescent-based model was defined with the same cortical and cancellous bone constant as the base modal, but with a Maxwell viscoelastic model of the growth plate (Fung 1993), (Humphrey and Delange 2004). Using a response based on a dashpot and spring in series, the stress equation becomes

$$\sigma(t) = 2 * [\varepsilon(0)G(t) + \int_{\tau=0}^{\tau=t} G(t-\tau)\frac{d\varepsilon(\tau)}{d\tau}d\tau]$$

where

$$G(t) = G_\infty + \sum_{n=1}^{N} G_n e^{(-t/\tau_n)}$$

The shear modulus is approximated by the two-term prony series

$$G(t) = 1 - G_1(1 - e^{t/\tau_1}) - G_2(1 - e^{t/\tau_2})$$

with $G_1 = 0.52$, $G_2 = 0.25$, $\tau_1 = 0.01$, $\tau_2 = 0.021$ (Clack, Ewers et al. 2002). It should be noted that this series is for bovine metacarpal cartilage.

4.2.2 Loading Conditions

One tremendous benefit of Abaqus is that it allows for static, quasi-static, and dynamic simulations. In this case, Abaqus/Explicit was used to create a quasi-static loading of the tibia based on the mathematical analysis in the previous chapter. Since it is a speed more applicable to athletic activities, the fastest speed of the Kanehisa study - 5.24 radians (300°) per second - was used, resulting in a total load time of three hundred msec. The load values for the tangential and normal components of the patellar tendon force were derived and input separately to account for the fact that the

patellar tendon insertion angle changes as the lower leg flexes and extends (Blackburn and Padua 2007).

In order to obtain an idea of how different activities might produce varying stresses and strains in the tibia, the forces estimated from an Autolev code for a jump take-off was added as a general comparison as to how different activities influence stress and strain. Just under 3000 linear tetrahedral (C3D4) elements were generated on the mesh of the tibia. Field output was requested at ten evenly spaced intervals, and included all stress and strain components.

4.3 Results

4.3.1 von Mises Stresses

The stress states in the various tibial models with will differ, even if they undergo the same loading. The stress tensor, which is used to fully describe the stress state, has six degrees of freedom, so it produces six independent components. As a result, it can be difficult to tell which of the models is more likely to exceed its failure point first. Von Mises stresses are a particularly useful alternative in determining the stress combination at points or sections of complex three-dimensional objects subjected to multiaxial loads. The von Mises criterion is able to use stress components to make predictions about where yielding or failure might occur. The criterion can be calculated in terms of the stress tensor components as

$$\sqrt{\frac{(\sigma_{11}-\sigma_{22})^2+(\sigma_{22}-\sigma_{33})^2+(\sigma_{33}-\sigma_{11})^2+6(\sigma_{12}^2+\sigma_{23}^2+\sigma_{31}^2)}{2}}$$

and compared with the material's ultimate stress.

In both the 'stronger' (adult) and 'weaker' (youth/adolescent) models of the tibia with dynamometer loading, the largest stress values occurred in the posterior portion, with the stress values slightly higher in the stronger material model. However, as mentioned in chapter 2, the ultimate strength of adolescent bone is below that of adults, and less resilient than that of children, it will reach the damage threshold more quickly, and therefore will be able to absorb less energy before fracturing (Bright, Burstein et al. 1974), (Chung 1976; Williams, Do et al. 2001). Figure 19 and Figure 20 depict stress distributions in the stronger and weaker models.

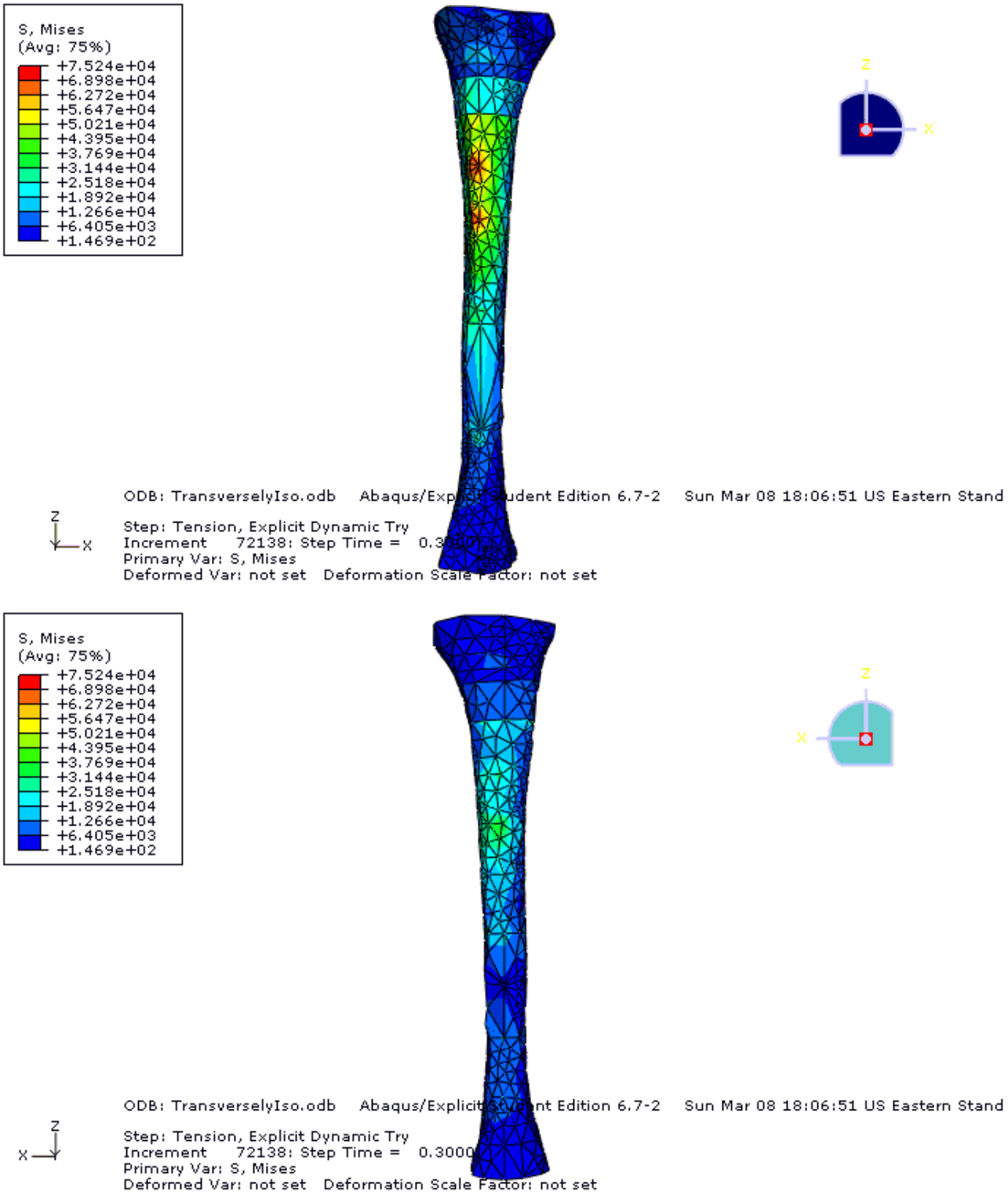

Figure 19. Posterior (top) and anterior views of von Mises stress contour plots on transversely isotropic growth plate model.

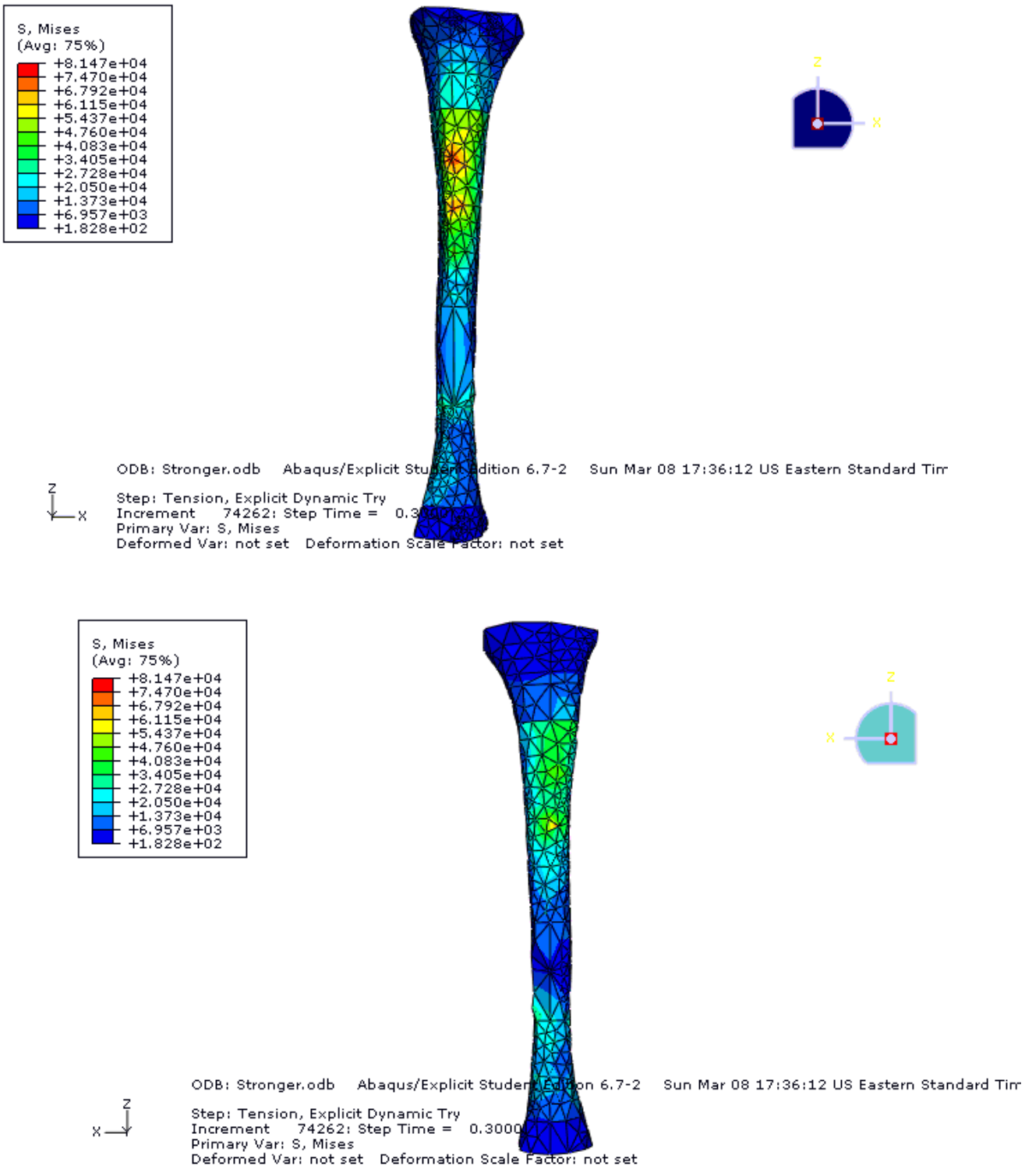

Figure 20. Posterior (top) and anterior views of mises stress contour plots for the stronger transversely isotropic model (no growth plate).

The locations of these stresses are of particular note, as fractures initiated in or traversing through the posterior aspect of tibia have the potential to damage the popliteal artery, which provides necessary nutrients for growth in the physeal plate and the surrounding bone (Figure 21).

4.3.2 Strain and Shear Stress

The strain profiles for the two models are less similar, both in value and in location (Figure 22). Maximum strains were 0.40 and 0.035 for the weaker/adolescent and stronger/adult models, respectively. In addition, the strain is localized in the growth plate region in the weaker material model, whereas there is a more gradual and spread out strain in the stronger material model.

The location of maximum shear is also an important quantity to consider, and scales with the quantity

$$\frac{|\sigma_1 - \sigma_3|}{2}$$

where σ_1 and σ_3 are the maximum and minimum principal stresses, respectively. The maximum principal stress is at a maximum on the anteromedial portion of the tibia (Figure 23). This location suggests a tendency towards type II and IV fractures, as depicted in the Salter-Harris classification illustration in Figure 2.

4.3.3 Viscoelastic Comparison

The adolescent model with the viscoelastic growth plate shows lower stress values in all areas than both the transversely isotropic growth plate model and the stronger model (Figure 24). In addition, elevated strain levels are confined to the anterior portion of the proximal tibia in the viscoelastic model, as opposed to higher strains extending all around the growth plate in the 'weaker' model (where the highest strain was in the anteromedial portion). This coincides with the suggestion that the growth plate becomes more vulnerable as it transitions from cartilage to adult bone.

4.3.4 Jump Take-Off Comparison

The stress and strain values of the jump takeoff and the baseline models are, as one would expect, quite different (Figures 25, 26). The jump take-off model shows a wider stress distribution, and reaches lower maximum stresses. Strain values are also lower by a

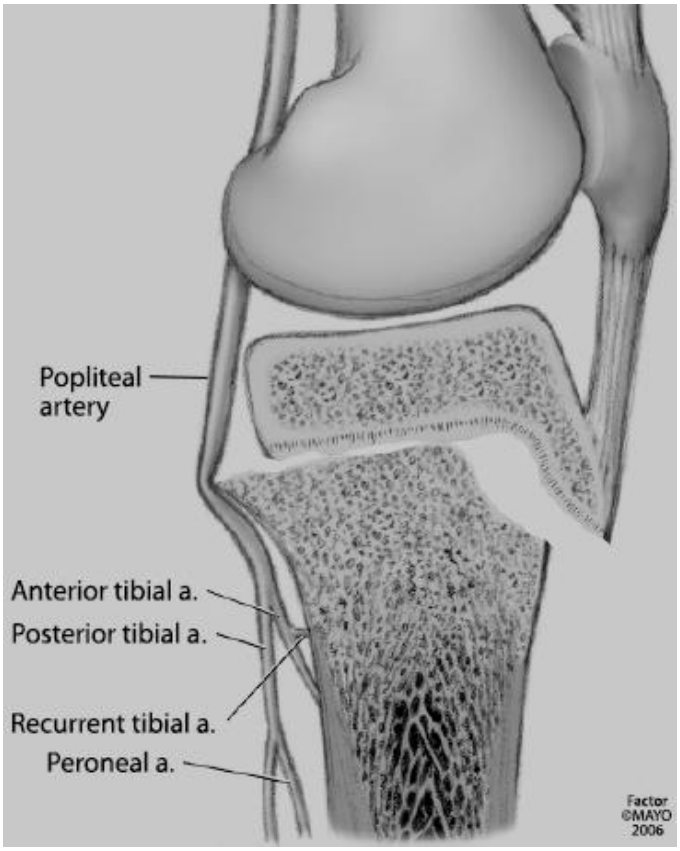

Figure 21. Impingement of popliteal artery from fractured physis (Peterson 2007).

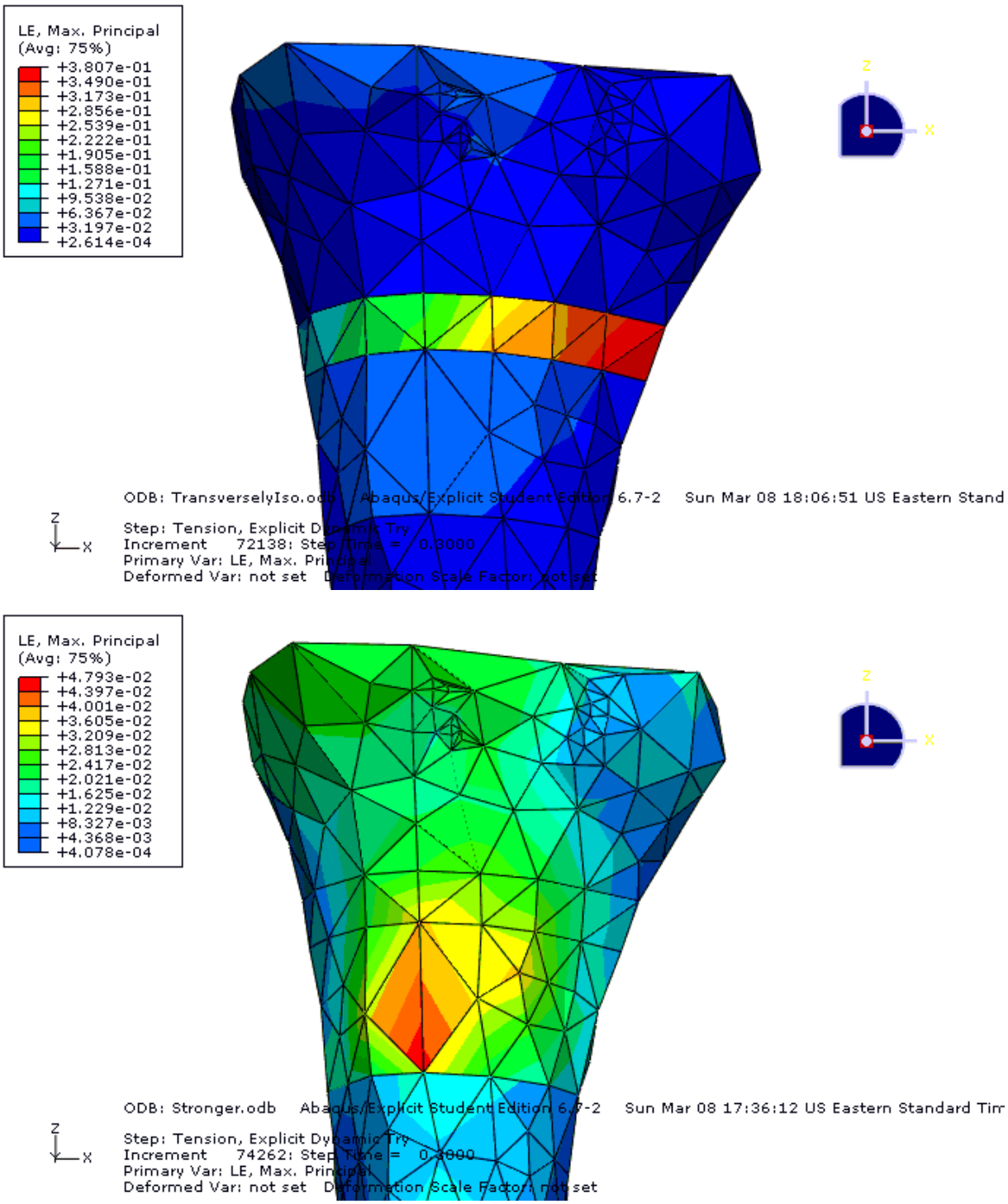

Figure 22. Posterior strain in the transversely isotropic growth plate (top) and stronger models. Contours of anterior strain are located in the appendix.

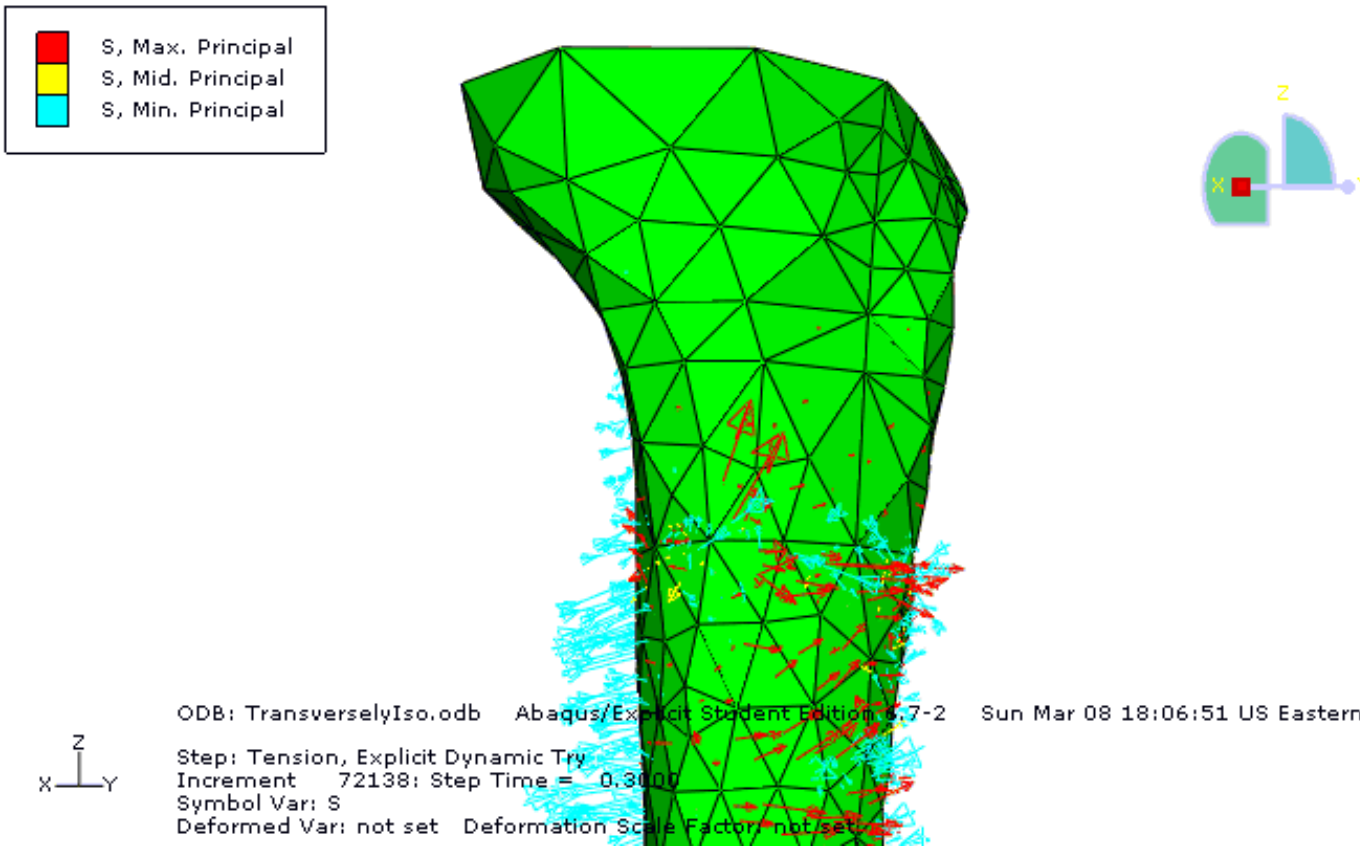

Figure 23. Vector representation of maximum (red) and minimum (blue) principal stresses.

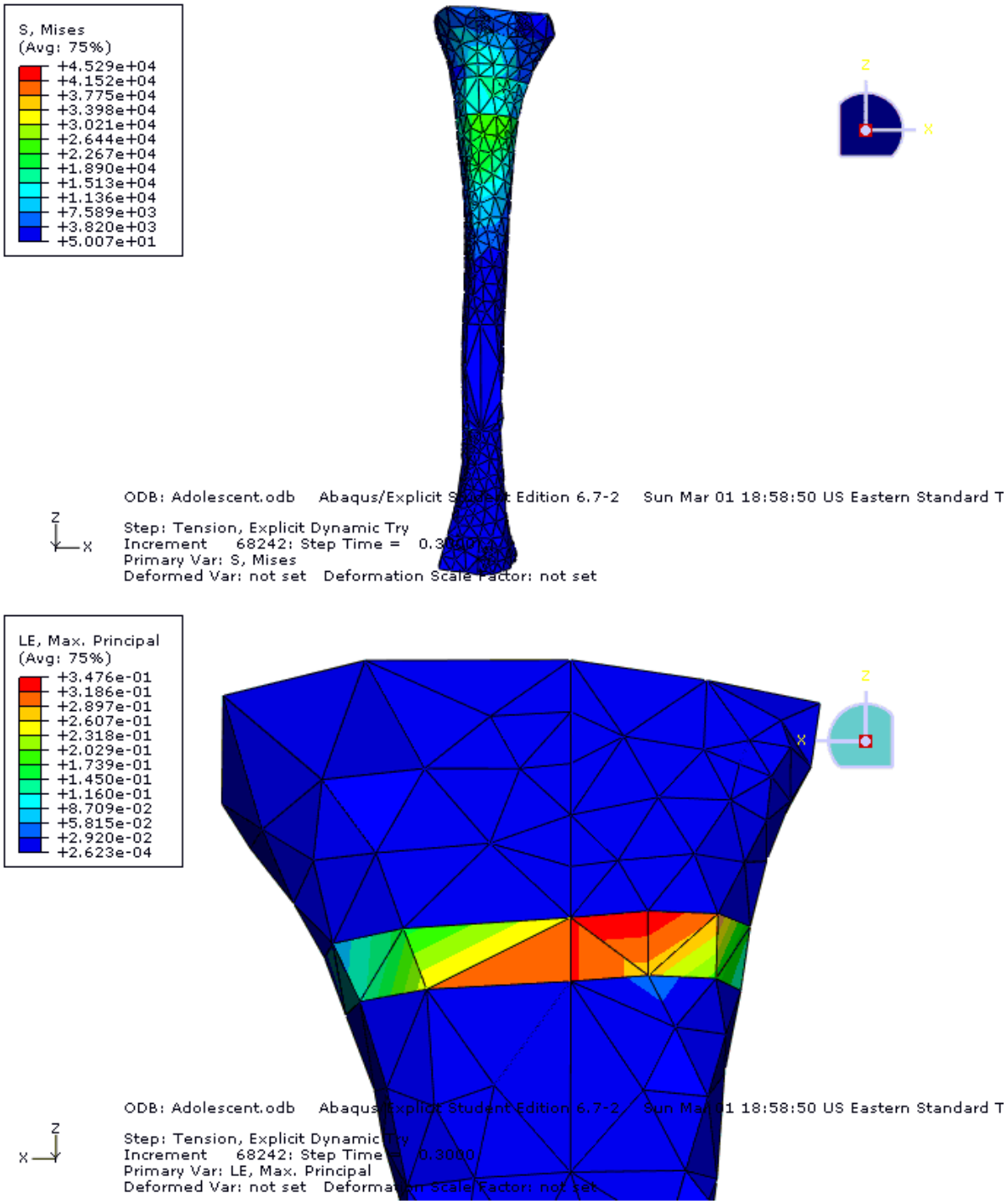

Figure 24. Viscoelastic model posterior stress (top) and anterior strain. Contours of anterior stress and posterior strain are located in the append

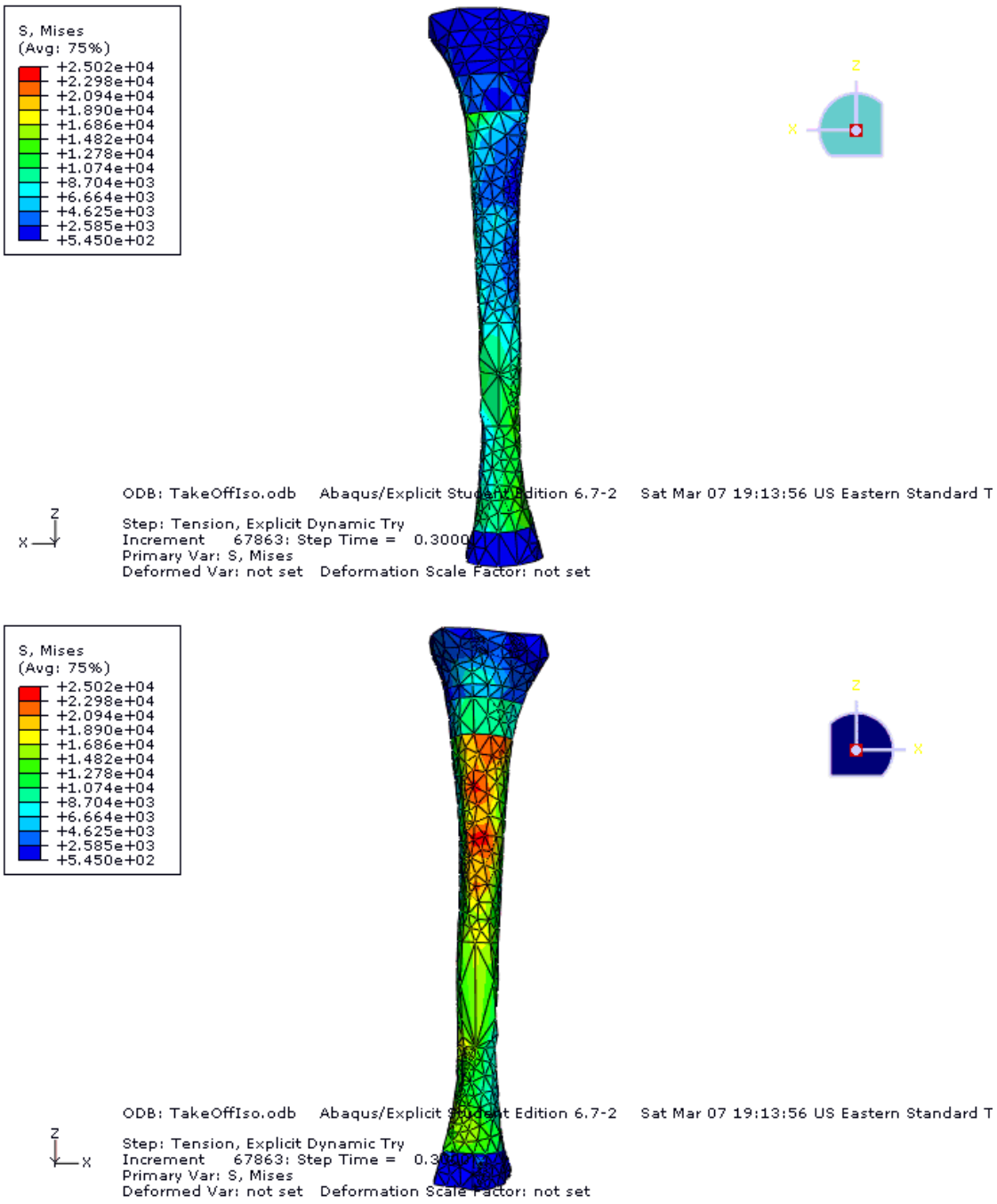

Figure 25. Jump take-off anterior (top) and posterior mises stress.

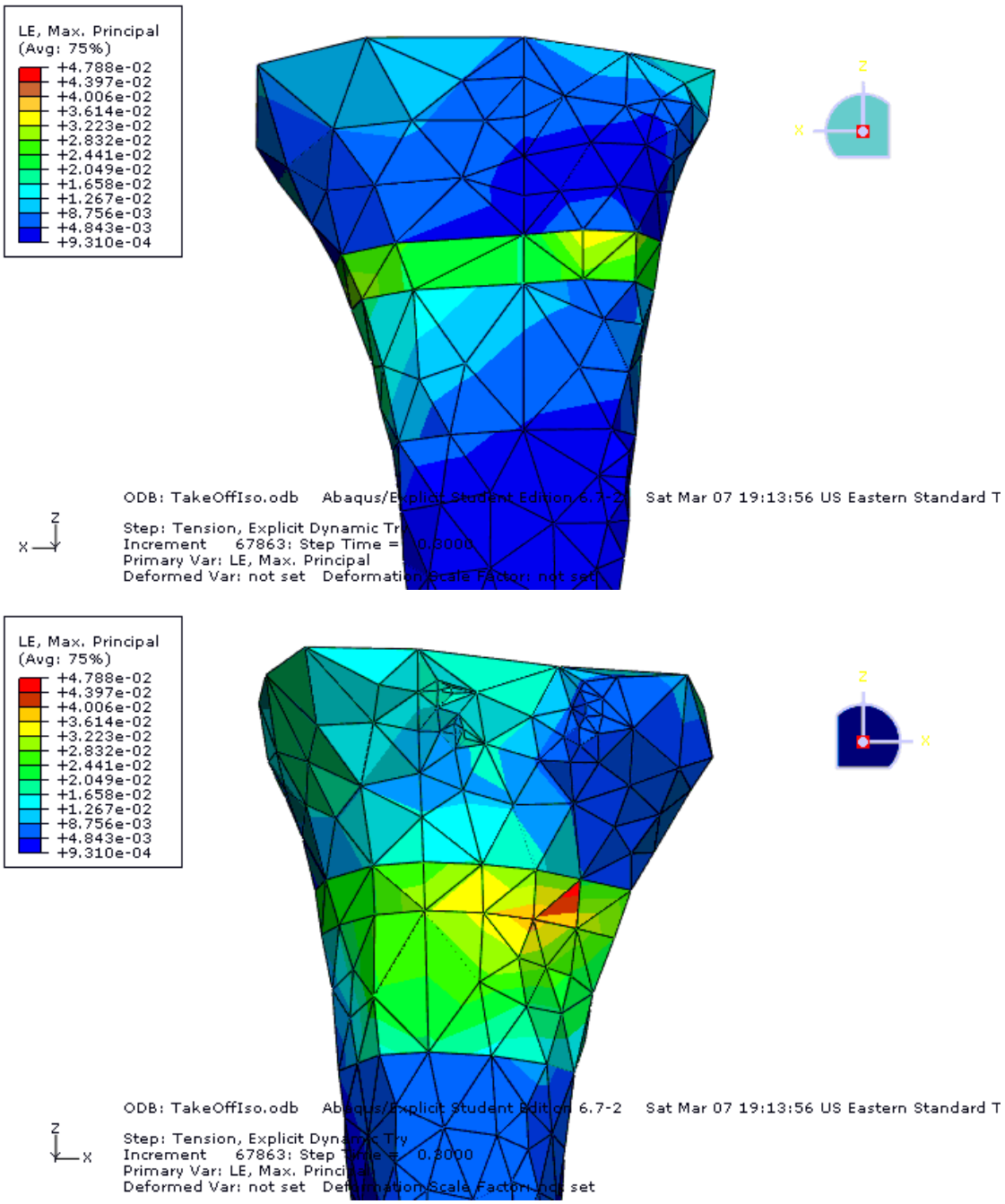

Figure 26. Jump take-off anterior (top) and posterior strain.

factor of ten, and are slightly localized in the growth plate anteriorly, and more widely distributed posteriorly. These results, however, should be considered in context, as the loading values did not include the action of the hamstrings, which may increase or decrease the stresses and strains. It seems likely that due to the efficiency and design of the body, addition of hamstring activity would counteract the force and therefore stress and strain values.

4.4 Summary

In terms of material properties, susceptibility of adolescent long bones to growth plate injuries is less likely the result of by the cartilaginous nature of the growth plate than the reduced strength of the growth plate and adjacent bone. This because of the maximum stress locations at the metaphysis, not the growth plate itself, and because of lower overall values in the viscoelastic model. As children progress into adolescence, the thickness of the growth plate increases, and its cartilaginous properties decrease. In addition, the bone loses some of its ability to absorb energy, but is not yet strong enough to withstand the higher loadings. For example, between the ages of six and fourteen, work absorption decreases by $5.6*10^{-3}$ J/m^2, while bending strength increases by 23 MN/m^2 between age fourteen and twenty-six. (Chung 1976), (Currey 1975). This analysis – strain and shear stress in particular - suggests that the most likely fracture location for extension movements would be either in the mid-posterior or slightly anterior medial portion of the metaphysis.

CHAPTER V: FUTURE CONSIDERATIONS AND CONCLUSIONS

The major differences in stress and strain locations and variations in magnitude underline the need to develop more specific models for various sports, as well as better description of the material properties of bone and growth plate, particularly in younger populations. The forces produced from the quadriceps and femorotibial contact are likely different during movements occurring over short periods such as jumps and cuts. This is an important aspect to consider, particularly in light of the Russel study (2007) that suggested differences in forces and impulse in landing between children and adults. However, some of this was accounted for by incorporating differing dynamometer force in the models. Also, this analysis was able to simulate dynamic, short loading rates, and may still be considered representative of the overall differences in loads and stresses in adults, children, and adolescents. Future studies can build on the initial survey of factors presented here by adding degrees of complexity and specificity.

5.1 Mathematical Model

One future goal is to develop three-dimensional mathematical models of the forces experienced during other lower body activities such as running and jumping, as well as for activities at different joints, e.g. pitching for the shoulder and elbow. For these activities, three-dimensional analyses are requisite for obtaining forces, since they consist of movements potentially occurring in the frontal, sagittal, and transverse planes. These models would also need to include the actions of several muscles. For example, an analysis of the shoulder might need to include the actions of the deltoid, teres minor, infraspinatus, and supraspinatus muscles, among others. In cases such as these, some assumptions similar to those made in this paper might need to be made to decrease the number of unknowns - that two muscles can be grouped together, or that certain muscle contributes to the movement are negligible.

Research data from gait analyses, pitching analyses, and force plates could be used in formulating such models and for generating data to input into Autolev codes for more individualized results. These models could then be useful first steps in screening for adolescents at increased risk for physeal fractures.

5.2 FE Model

Future models could also build increasing amounts of complexity into a finite element analysis, which would ideally incorporate mechanical property tests to define more specific material behavior. Along these lines, it may also be beneficial to perform analysis on and characterize the behavior of the different growth plate zones, since they have different compositions and/or compositional organizations (i.e. the scattered cells in the reserve zone versus the aligned cells in the hypertrophic zone) that may affect how they respond to different loading patterns.

Inclusion of soft tissues, the patella, and femur would also give a more holistic result of the stresses and interactions of the model as well. This could be accelerated through the use of CT and MRI scanning, with software capable of generating 3D images that are importable into finite element packages such as Abaqus™. Such a model could then be scaled to correlate to individual adolescents, reducing the necessity of exposure to x-rays. The finite element model could be used as a supplement to the mathematical model, and use force and moment values obtained from that analysis to suggest which activities, when overdone, are more likely to lead to pain or injury, and which activities can provide a 'break' to the at-risk area.

5.3 Future Considerations

Further studies may also wish to focus more exclusively on one of the aspects identified here, and perform a more in-depth analysis on the influence of that one particular factor. For example, since patellar tendon length appears to have a significant effect on proximal tibial loading, a study could investigate the correlation between the ratio of patellar ligament length to tibial/femur length, or quadriceps strength to leg length and occurrence of fractures.

In addition, one hypothesized factor in physeal injuries that was not covered in this paper is the difference in movement strategies between adults and children. This could include landing and jumping strategies in sports such as basketball and track and field, or throwing and swinging in baseball and tennis.

Case studies may also want to gradually focus on more specific factors as well. This includes recording information such as where the fracture initiates as well as

- What sport the athlete was playing at the time of fracture
- Whether the sport is played seasonally or on a year-round basis
- How many hours a week the athlete was training or competing in the sport, and if it had increased recently
- Other sports the adolescent plays competitively
- Change in growth from the last check-up

5.4 Conclusions

The main conclusion is that the occurrence of physeal fractures at the proximal tibia is a combination of

1) Increased force being transmitted through the patellar ligament, whether by increased muscle force, or because of a lag in the growth of patellar ligament with respect to the tibia.
2) Presence of weaker growth plate, and bone that is both less stiff and less able to absorb energy. This bone is, as a result, more susceptible to microfracture, and less able to remodel in time to accommodate increased load.

Since the growth process itself is necessary, along with its window of particular weakness, the focus turns to prevention through external factors, specifically the watchfulness of pediatricians, parents, and coaches. Although physical activity is vital for both health of the child and for the development of bone strength, these caretakers should become aware of the first signs of a growth spurt, and make several considerations concerning their young athlete. During periods of rapid growth, susceptibility to physeal fractures and other overuse injuries could be likely be lessened by:

- Avoiding rapid or sudden increases in training intensity or volume
- Utilizing training regimens that take care to work different muscle groups
- Engaging in a variety of sports and activities, avoiding training and playing for a single sport year-round

With the latter two suggestions varying loading profiles, and therefore potentially minimizing localized induced stresses and strains, injuries, and periods of inactivity.

REFERENCES

(2000). 2000 CDC Growth Charts: United States, Center for Disease Control.

Abbassi, V. (1998). "Growth and normal puberty." Pediatrics **102**(2): 507.

Abdel-Rahman, E. and M. S. Hefzy (1993). "A Two-Dimensional Dynamic Anatomical Model of the Human Knee Joint." Journal of Biomechanical Engineering **115**: 357.

Adirim, T. A. and T. L. Cheng (2003). "Overview of Injuries in the Young Athlete." Sports Medicine **33**(1): 75.

Alexander, C. J. (1976). "Effect of growth rate on the strength of the growth plate-shaft junction." Skeletal Radiology **1**(2): 67-76.

Alter, M. J. (2004). Science of Flexibility, Human Kinetics.

Anderson, F. C. and M. G. Pandy (2001). "Dynamic Optimization of Human Walking." Journal of Biomechanical Engineering **123**: 381.

Ardatov, N. (2006). "The Tibia ".

Baratz, M., A. D. Watson, et al. (1999). Orthopaedic Surgery: The Essentials, Thieme.

Blackburn, J. T. and D. A. Padua (2007). "Influence of trunk flexion on hip and knee joint kinematics during a controlled drop landing." Clinical Biomechanics.

Blankevoort, L. and R. Huiskes (1996). "Validation of a three-dimensional model of the knee." Journal of Biomechanics **29**(7): 955-961.

Bright, R. W., A. H. Burstein, et al. (1974). "Epiphyseal-Plate Cartilage: A BIOMECHANICAL AND HISTOLOGICAL ANALYSIS OF FAILURE MODES." The Journal of Bone and Joint Surgery **56**(4): 688.

Bundak, R., F. Darendeliler, et al. (2007). "Analysis of puberty and pubertal growth in healthy boys." European Journal of Pediatrics **166**(6): 595-600.

Burkhart, S. S. (1979). Fractures of the proximal tibial epiphysis, JBJS. **61:** 996-1002.

Caine, D., S. Roy, et al. (1992). "Stress changes of the distal radial growth plate: A radiographic survey and review of the literature." The American Journal of Sports Medicine **20**(3): 290.

Chung, S. M. (1976). Shear strength of the human femoral capital epiphyseal plate, JBJS. **58:** 94-103.

Clack, E., B. Ewers, et al. (2002). A HYPERVISCOELASTIC MODEL FOR UNCONFINED COMPRESSION OF ARTICULAR CARTILAGE UNDER IMPACT RATES OF LOADING.

Currey, J. D. (1975). The mechanical properties of bone tissue in children, JBJS. **57:** 810-814.

Dalton, S. E. (1992). "Overuse injuries in adolescent athletes." Sports Medicine **13**(1): 58-70.

D'Lima, D. D., S. Patil, et al. (2006). "Tibial forces measured in vivo after total knee arthroplasty." The Journal of arthroplasty **21**(2): 255-262.

Ford, C. M. and T. M. Keaveny (1996). "The dependence of shear failure properties of trabecular bone on apparent density and trabecular orientation." Journal of Biomechanics **29**(10): 1309-1317.

Fung, Y. C. (1993). Biomechanics: mechanical properties of living tissues, Springer.

Gómez-Benito, M. J., P. Moreo, et al. (2007). "A damage model for the growth plate: Application to the prediction of slipped capital epiphysis." Journal of Biomechanics **40**(15): 3305-3313.

Halloran, J. P., A. J. Petrella, et al. (2005). "Explicit finite element modeling of total knee replacement mechanics." Journal of Biomechanics **38**(2): 323-331.

Heller, M. O., G. Bergmann, et al. (2001). "Musculo-skeletal loading conditions at the hip during walking and stair climbing." Journal of Biomechanics **34**(7): 883-893.

Hoffmeister, B. K., S. R. Smith, et al. (2000). "Anisotropy of Young's modulus of human tibial cortical bone." Medical and Biological Engineering and Computing **38**(3): 333-338.

Humphrey, J. D. and S. L. Delange (2004). An introduction to biomechanics: solids and fluids, analysis and design, Springer.

Iannotti, J., S. Goldstein, et al. (2000). The Formation and Growth of Skeletal Tissues. Orthopaedic Basic Science: Biology and Biomechanics of the Musculoskeletal System. J. A. Buckwalter, T. A. Einhorn and S. R. Simon, American Academy of Orthopaedic Surgeons

Iuliano-Burns, S., R. L. Mirwald, et al. (2001). "Timing and magnitude of peak height velocity and peak tissue velocities for early, average, and late maturing boys and girls." American Journal of Human Biology **13**(1): 1-8.

Jensen, R. K. (1989). "Changes in segment inertia proportions between 4 and 20 years." J Biomech **22**(6-7): 529-36.

Kane, T. R. and D. A. Levinson (1983). "Multibody dynamics." ASME, Transactions, Journal of Applied Mechanics **50**(4): 1071-1078.

Kanehisa, H., H. Yata, et al. (1995). "A cross-sectional study of the size and strength of the lower leg muscles during growth." European Journal of Applied Physiology **72**(1): 150-156.

Kellis, E. (2001). "Tibiofemoral joint forces during maximal isokinetic eccentric and concentric efforts of the knee flexors." Clinical Biomechanics **16**(3): 229-236.

Komistek, R. D., J. B. Stiehl, et al. (1997). "Mathematical model of the lower extremity joint reaction forces using Kane's method of dynamics." Journal of Biomechanics **31**(2): 185-189.

Krueger-Franke, M., C. H. Siebert, et al. (1992). "Sports-related epiphyseal injuries of the lower extremity: an epidemiologic study." Journal of sports medicine and physical fitness **32**(1): 106-111.

Laor, T., E. J. Wall, et al. (2006). "Physeal Widening in the Knee Due to Stress Injury in Child Athletes." American Journal of Roentgenology **186**(5): 1260-1264.

Lian, O. B., L. Engebretsen, et al. (2005). "Prevalence of jumper's knee among elite athletes from different sports: a cross-sectional study." The American Journal of Sports Medicine **33**(4): 561.

Macdonald, H., S. Kontulainen, et al. (2006). "Bone strength and its determinants in pre-and early pubertal boys and girls." Bone **39**(3): 598-608.

Macdonald, H. M., S. A. Kontulainen, et al. (2005). "Maturity-and sex-related changes in tibial bone geometry, strength and bone–muscle strength indices during growth: A 20-month pQCT study." Bone **36**(6): 1003-1011.

Martin, R. B., D. B. Burr, et al. (1998). Skeletal Tissue Mechanics. New York, Springer.

McKay, H., G. Tsang, et al. (2005). Ground reaction forces associated with an effective elementary school based jumping intervention, BASM. **39:** 10-14.

Micheli, L. J. (1986). "Pediatric and adolescent sports injuries: recent trends." Exerc Sport Sci Rev **14**: 359-74.

Mirbey, J., J. Besancenot, et al. (1988). "Avulsion fractures of the tibial tuberosity in the adolescent athlete: Risk factors, mechanism of injury, and treatment." The American Journal of Sports Medicine **16**(4): 336.

Niemeyer, P., A. Weinberg, et al. (2006). "Stress fractures in adolescent competitive athletes with open physis." Knee Surgery, Sports Traumatology, Arthroscopy **14**(8): 771-777.

Nisell, R., M. O. Ericson, et al. (1989). "Tibiofemoral joint forces during isokinetic knee extension." The American Journal of Sports Medicine **17**(1): 49.

Osternig, L. R., J. Hamill, et al. (1984). "Electromyographic patterns accompanying isokinetic exercise under varying speed and sequencing conditions." American journal of physical medicine **63**(6): 289-297.

Peterson, H. A. (2007). Epiphyseal growth plate fractures, Springer

Radhakrishnan, P., N. T. Lewis, et al. (2004). "Zone-Specific Micromechanical Properties of the Extracellular Matrices of Growth Plate Cartilage." Annals of Biomedical Engineering **32**(2): 284-291.

Rauch, F., D. A. Bailey, et al. (2004). "The 'muscle-bone unit'during the pubertal growth spurt." Bone **34**(5): 771-775.

Russell, P. J., R. V. Croce, et al. (2007). "Knee-Muscle Activation during Landings: Developmental and Gender Comparisons." Medicine & Science in Sports & Exercise **39**(1): 159.

Sairyo, K., V. K. Goel, et al. (2006). "Three dimensional finite element analysis of the pediatric lumbar spine. Part II: biomechanical change as the initiating factor for pediatric isthmic spondylolisthesis at the growth plate." European Spine Journal **15**(6): 930-935.

Sairyo, K., V. K. Goel, et al. (2006). "Three-dimensional finite element analysis of the pediatric lumbar spine. Part I: pathomechanism of apophyseal bony ring fracture." European Spine Journal **15**(6): 923-929.

Salter, R. B. and W. R. Harris (1963). "Injuries Involving the Epiphyseal Plate." The Journal of Bone and Joint Surgery **45**(3): 587.

Wheeless, C. R. (1996). Wheeless'Textbook of Orthopaedics. Duke University Medical Center
Division of Orthopaedic Surgery, DataTrace Internet Pub.

Williams, J. L., P. D. Do, et al. (2001). "Tensile properties of the physis vary with anatomic location, thickness, strain rate and age." Journal of Orthopaedic Research **19**(6): 1043-1048.

Yoon, Y. J., G. Yang, et al. (2002). "Estimation of the effective transversely isotropic elastic constants of a material from known values of the material's orthotropic elastic constants." Biomechanics and Modeling in Mechanobiology **1**(1): 83-93.

APPENDICES

Appendix A. Autolev Codes, Outputs, and Graphs

A.1 Autolev Code (adult with dynamometer force)

```
_____
**************************************************************************************************
%% MATHEMATICAL MODEL OF ADULT MALE LEG EXTENSION
%
%% 2DADULT.AL
%%
%% ASSUMPTIONS: 2D
%
%%       LEFT LEG
%                  _________ N2>
%%              |
%%              |
%%              |
%%              |
%%              | N1>
%%
%
%
%% 3 AXIS ROTATIONS
NEWTONIAN N
BODIES A
FRAMES B
% ROTATION ANGLES
SPECIFIED Q{2}''
%
% GENERALIZED SPEEDS
%
VARIABLES U{6}'
%
% UNKNOWN FORCES
%
VARIABLES FNA{2},FAB, FAB_A1, FAB_A2
%
% POINTS ON FEMUR
%
POINTS NA
%
% POINTS ON TIBIA
%
POINTS AN,AB,AC
%
% POINTS ON PATELLAR LIGAMENT
```

Appendix A.1 Continued

```
%
POINTS BA
%
%% TIBIAL LENGTH, DISTANCE FROM
%% INSERTION OF PATELLAR LIGAMENT,
%% CENTER OF MASS TO END OF TIBIA,
%% AND HALF THE LENGTH OF THE PATELLAR TENDON
%
CONSTANTS ANAC1, ANAB{2}, AOAC1, BABO{2}
%
%% BODY WEIGHT, FOOT WEIGHT,
%% SUBJECT HEIGHT, DYNAMOMETER FORCE
%
CONSTANTS BM, BW, FOOT, HEIGHT, F_D
%
%% DEFINE MASSES, INERTIA, & GRAVITY
%
G=9.81
MASS A=(0.046*BW)/G
GRAVITY(G*N1>)
INERTIA A,0,0,KA3
KA3=(0.046*BW)/G*(ANAC1-AOAC1)^2
%
FOOT=0.014*BW
%
%% DEFINE ANGLE ROTATIONS
%
%
Q1 = -1.05*T
Q2 = (8*PI/15) - (7*PI/90)*T
%
%% SIMPLE ROTATIONS
%
SIMPROT(N,A,3,Q1)
SIMPROT(A,B,3,Q2)
%
%% ANGULAR VELOCITY
%
W_A_N>=W_A_N>+U1*A3>
%
%% POSITION VECTORS
%
L_TIBIA=0.233*HEIGHT
ANAC1=L_TIBIA
AOAC1=ANAC1*0.57
%
P_NO_NA>=0>
```

Appendix A.1 Continued

```
P_NA_AN>=0>
P_AN_AB> = ANAB1*A1> - ANAB2*A2>
P_AN_AC> = ANAC1*A1>
P_AO_AC> = AOAC1*A1>
P_AB_BA>=0>
P_BA_BO> = BABO2*B2>
%
%
%% VELOCITIES
%
V_NO_N>=0>
V_NA_N>=0>
V_AN_N>= V_NA_N> + U2*A1> + U3*A2>
V2PTS(N,A,AN,AO)
V2PTS(N,A,AN,AB)
V2PTS(N,A,AN,AC)
V2PTS(N,B,AB,BA)
V2PTS(N,B,BA,BO)
%
%
AUXILIARY[1]=U1
AUXILIARY[2]=U2
AUXILIARY[3]=U3
%
CONSTRAIN(AUXILIARY[U1,U2,U3])
%
%
FORCE(NA/AN, FNA1*A1> + FNA2*A2>)
FORCE_AB>=FAB*B2>
FORCE_AC>=FOOT*N1> + F_D*A2>
FAB_A1=FAB*DOT(B2>,A1>)
FAB_A2=FAB*DOT(B2>,A2>)
%
%
ZERO=FR()+FRSTAR()
KANE(FNA1,FNA2, FAB)
%
%% INPUT AND OUTPUT FILE GENERATION
%
%  PATELLAR TENDON LENGTHS
INPUT ANAB1=0.032,ANAB2= 0.025
INPUT BABO2=0.15
%
% BODY WEIGHT AND HEIGHT
%
INPUT Bw=850,HEIGHT=1.7
%
```

Appendix A.1 Continued

```
DYNAMOMETER FORCE
%
INPUT F_D=472.1
OUTPUT T,Q1,Q2
OUTPUT t, FNA1,FNA2
OUTPUT t, FAB, FAB_A1, FAB_A2
OUTPUT t, FNA1/BW,FNA2/BW
OUTPUT t, FAB/BW, FAB_A1/BW, FAB_A2/BW
%
%% ANIMATION AND FORTRAN CODE GENERATION
%
ANIMATE(N,NO,A,B)
CODE ALGEBRAIC () [T=0,1.5,0.01] 2DADULT.FOR
**********************************************************************************************
```

A.2 Autolev Output File (13 year-old) .

The arrows indicate calculations performed by Autolev.

```
_____
********************************************************************************
  (1) %% MATHEMATICAL MODEL OF 13 Y/O YOUTH LEG EXTENSION
  (2) %
  (3) %% 13.AL
  (4) %
  (5) %%
  (6) %
  (7) %% ASSUMPTIONS: 2D
  (8) %
  (9) %%        LEFT LEG
  (10) %                    _________ N2>
  (11) %%                  |
  (12) %%                  |
  (13) %%                  |
  (14) %%                  |
  (15) %%                  | N1>
  (16) %%
  (17) %
  (18) %% 3 AXIS ROTATIONS
  (19)_____________________________________________________________________
  (20) %
  (21) NEWTONIAN N
  (22) BODIES A
  (23) FRAMES B
  (24) SPECIFIED Q{3}''
  (25) VARIABLES U{6}'
  (26) VARIABLES FNA{2},FAB
  (27) %
  (28) POINTS NA,AN,AB,BA,AC,
  (29) CONSTANTS ANAC1, ANAB{2}, AOAC1,BABO{2},
  (30) CONSTANTS BM, BW, FOOT, HEIGHT, F_D
  (31) %

  (32) G=9.81
-> (33) G = 9.81

  (34) MASS A=(0.054*BW)/G

  (35) GRAVITY(G*N1>)
-> (36) FORCE_AO> = 0.054*BW*N1>

  (37) INERTIA A,0,0,KA3
```

Appendix A.2 Continued

```
-> (38) I_A_AO>> = KA3*A3>*A3>

   (39) %

   (40) KA3 = (0.054*BW)/G*(ANAC1-AOAC1)^2
-> (41) KA3 = 0.005504587*BW*(ANAC1-AOAC1)^2

   (42) %

   (43) FOOT=0.02065*BW
-> (44) FOOT = 0.02065*BW

   (45) %
   (46) DEGREES OFF
   (47) %

   (48) Q1 = -1.05*T
-> (49) Q1 = -1.05*T

   (50) Q2 = (8*PI/15) - (7*PI/90)*T
-> (51) Q2 = 1.675516 - 0.2443461*T

   (52) %
   (53) %% SIMPLE ROTATIONS
   (54) %

   (55) SIMPROT(N,A,3,Q1)
-> (56) N_A = [COS(Q1), -SIN(Q1), 0; SIN(Q1), COS(Q1), 0; 0, 0, 1]

   (57) SIMPROT(A,B,3,Q2)
-> (58) A_B = [COS(Q2), -SIN(Q2), 0; SIN(Q2), COS(Q2), 0; 0, 0, 1]

   (59) %
   (60) %% ANGULAR VELOCITY
   (61) %

   (62) W_A_N>=W_A_N>+U1*A3>
-> (63) W_A_N> = (Q1'+U1)*A3>

   (64) %
   (65) %% POSITION VECTORS
   (66) %
   (67) L_TIBIA=0.233*HEIGHT
-> (68) L_TIBIA = 0.233*HEIGHT
   (69) ANAC1=L_TIBIA
-> (70) ANAC1 = L_TIBIA
   (71) AOAC1=ANAC1*0.5964
```

Appendix A.2 Continued

-> (72) AOAC1 = 0.5964*ANAC1

(73) %
(74) P_NO_NA>=0>
-> (75) P_NO_NA> = 0>
(76) P_NA_AN>=0>
-> (77) P_NA_AN> = 0>
(78) P_AN_AB> = ANAB1*A1> - ANAB2*A2>
-> (79) P_AN_AB> = ANAB1*A1> - ANAB2*A2
(80) P_AN_AC> = ANAC1*A1>
-> (81) P_AN_AC> = ANAC1*A1>
(82) P_AO_AC> = AOAC1*A1>
-> (83) P_AO_AC> = AOAC1*A1>
(84) P_AB_BA>=0>
-> (85) P_AB_BA> = 0>
(86) P_BA_BO> = BABO2*B2>
-> (87) P_BA_BO> = BABO2*B2>

(88) %
(89) %
(90) %% VELOCITIES
(91) %
(92) V_NO_N>=0>
-> (93) V_NO_N> = 0>

(94) V_NA_N>=0>
-> (95) V_NA_N> = 0>

(96) V_AN_N>= V_NA_N> + U2*A1> + U3*A2>
-> (97) V_AN_N> = U2*A1> + U3*A2>

(98) V2PTS(N,A,AN,AO)
-> (99) V_AO_N> = U2*A1> + (U3+(ANAC1-AOAC1)*(Q1'+U1))*A2>

(100) V2PTS(N,A,AN,AB)
-> (101) V_AB_N> = (U2+ANAB2*(Q1'+U1))*A1> + (U3+ANAB1*(Q1'+U1))*A2>

(102) V2PTS(N,A,AN,AC)
-> (103) V_AC_N> = U2*A1> + (U3+ANAC1*(Q1'+U1))*A2>

(104) V2PTS(N,B,AB,BA)
-> (105) V_BA_N> = (U2+ANAB2*(Q1'+U1))*A1> + (U3+ANAB1*(Q1'+U1))*A2>

(106) V2PTS(N,B,BA,BO)
-> (107) V_BO_N> = (U2+ANAB2*(Q1'+U1))*A1> + (U3+ANAB1*(Q1'+U1))*A2> - BABO2*(Q1'+Q2'+U1)*B1>

Appendix A.2 Continued

```
   (108) %
   (109) AUXILIARY[1]=U1
-> (110) AUXILIARY[1] = U1
   (111) AUXILIARY[2]=U2
-> (112) AUXILIARY[2] = U2
   (113) AUXILIARY[3]=U3
-> (114) AUXILIARY[3] = U3

   (115) %
   (116) CONSTRAIN(AUXILIARY[U1,U2,U3])
-> (117) U1 = 0
-> (118) U2 = 0
-> (119) U3 = 0
-> (120) U1' = 0
-> (121) U2' = 0
-> (122) U3' = 0

   (123) %
   (124) FORCE(NA/AN, FNA1*N1> + FNA2*N2>)
-> (125) FORCE_AN> = FNA1*N1> + FNA2*N2>
-> (126) FORCE_NA> = -FNA1*N1> - FNA2*N2>

   (127) FORCE_AB>=FAB*B2>
-> (128) FORCE_AB> = FAB*B2>

   (129) FORCE_AC>=FOOT*N1> + F_D*A2>
-> (130) FORCE_AC> = F_D*A2> + FOOT*N1>

   (131) %
   (132) %
   (133) ZERO=FR()+FRSTAR()

-> (134) ZERO[1] = 0

-> (135) ZERO[2] = 0

-> (136) ZERO[3] = 0

-> (137) ZERO[4] = ANAC1*(F_D-FOOT*SIN(Q1)) + (ANAB1*COS(Q2)-
ANAB2*SIN(Q2))*FAB- 0.054*BW*(ANAC1-AOAC1)*SIN(Q1) -
0.005504587*(181.6667*KA3+BW*(ANAC1-AOAC1)^2)*Q1"

-> (138) ZERO[5] = FOOT*COS(Q1) + 0.054*BW*COS(Q1) +
0.005504587*BW*(ANAC1-AOAC1)*Q1'^2 + SIN(Q1)*FNA2 + COS(Q1)*FNA1 -
SIN(Q2)*FAB
```

Appendix A.2 Continued

-> (139) ZERO[6] = F_D + COS(Q1)*FNA2 + COS(Q2)*FAB - FOOT*SIN(Q1) - 0.054*BW*SIN(Q1) - 0.005504587*BW*(ANAC1-AOAC1)*Q1'' - SIN(Q1)*FNA1

(140) KANE(FNA1,FNA2, FAB)

-> (141) FNA1 = 0.005504587*SIN(Q1)*(181.6667*F_D-181.6667*FOOT*SIN(Q1)-9.81*BW*SIN(Q1)-BW*(ANAC1-AOAC1)*Q1''-COS(Q2)*(181.6667*ANAC1*(F_D-FOOT*SIN(Q1))-9.81*BW*(ANAC1-AOAC1)*SIN(Q1)-(181.6667*KA3+BW*(ANAC1-AOAC1)^2)*Q1'')/(ANAB1*COS(Q2)-ANAB2*SIN(Q2))) - 0.005504587*COS(Q1)*(9.81*BW* COS(Q1)+181.6667*FOOT*COS(Q1)+BW*(ANAC1-AOAC1)*Q1'^2+SIN(Q2)*(181.6667*ANAC1*(F_D-FOOT*SIN(Q1))-9.81*BW*(ANAC1-AOAC1)*SIN(Q1)-(181.6667*KA3+BW*(ANAC1-AOAC1)^2)*Q1'')/(ANAB1*COS(Q2)-ANAB2*SIN(Q2)))

-> (142) FNA2 =- 0.005504587*SIN(Q1)*(9.81*BW*COS(Q1)+181.6667*FOOT*COS(Q1)+BW*(ANAC1-AOAC1)*Q1'^2+SIN(Q2)*(181.6667*ANAC1*(F_D-FOOT*SIN(Q1))-9.81*BW*(ANAC1-AOAC1)*SIN(Q1)-(181.6667*KA3+BW*(ANAC1-AOAC1)^2)*Q1'')/(ANAB1*COS(Q2)-ANAB2*SIN(Q2))) - 0.005504587*COS(Q1)*(181.6667*F_D-181.6667*FOOT*SIN(Q1)-9.81*BW*SIN(Q1)-BW*(ANAC1-AOAC1)*Q1''-COS(Q2)*(181.6667*ANAC1*(F_D-FOOT*SIN(Q1))-9.81*BW*(ANAC1-AOAC1)*SIN(Q1)-(181.6667*KA3+BW*(ANAC1-AOAC1)^2)*Q1'')/(ANAB1*COS(Q2)-ANAB2*SIN(Q2)))

-> (143) FAB = -0.005504587*(181.6667*ANAC1*(F_D-FOOT*SIN(Q1))-9.81*BW*(ANAC1- AOAC1)*SIN(Q1) - (181.6667*KA3+BW*(ANAC1-AOAC1)^2)*Q1'')/(ANAB1*COS(Q2) - ANAB2*SIN(Q2))

-> (144) ZERO[1] = 0

-> (145) ZERO[2] = 0

-> (146) ZERO[3] = 0
(147) %
(148) INPUT ANAB1=0.0294,ANAB2= 0.0229
(149) INPUT BABO2=0.137
(150) INPUT BW=450,HEIGHT=1.56
(151) INPUT F_D= 250
(152) OUTPUT T,Q1,Q2
(153) OUTPUT Q1, FNA1,FNA2
(154) OUTPUT Q1, FAB
(155) %
(156) ANIMATE(N,NO,A,B)

-> (157) P_NO_AO = [(ANAC1-AOAC1)*COS(Q1); (ANAC1-AOAC1)*SIN(Q1); 0]

-> (158) P_NO_BO[1] = ANAB1*COS(Q1) + ANAB2*SIN(Q1) - BABO2*SIN(Q1+Q2)

Appendix A.2 Continued

-> (159) P_NO_BO[2] = ANAB1*SIN(Q1) + BABO2*COS(Q1+Q2) - ANAB2*COS(Q1)

-> (160) P_NO_BO[3] = 0

-> (161) N_B = [COS(Q1+Q2), -SIN(Q1+Q2), 0; SIN(Q1+Q2), COS(Q1+Q2), 0; 0, 0, 1]

(162) CODE ALGEBRAIC () [T=0,1.5,0.01] 13.FOR

-> (163) Q1' = -1.05
-> (164) Q1'' = 0
-> (165) Q2' = -0.2443461
-> (166) Q2'' = 0

A.3 Fortan code for the slow adult model

```
_____________________________________________________________________________________________
**********************************************************************************************
C**   The name of this program is 2dadult.for
C**   Created by Autolev 4.0 on Thu Jan 29 19:00:48 2009
C**   MATHEMATICAL MODEL OF ADULT MALE LEG EXTENSION
C**   2DADULT.AL
C**
C**   ASSUMPTIONS: 2D
C**   LEFT LEG
C**   |
C**   |
C**   |
C**   |
C**   | N1>
C**
C**   3 AXIS ROTATIONS
C**   TIBIAL LENGTH, DISTANCE FROM
C**   INSERTION OF PATELLAR LIGAMENT,
C**   CENTER OF MASS TO END OF TIBIA,
C**   AND HALF THE LENGTH OF THE PATELLAR TENDON
C**   BODY WEIGHT, FOOT WEIGHT,
C**   SUBJECT HEIGHT, DYNAMOMETER FORCE
C**   DEFINE MASSES, INERTIA, & GRAVITY
C**   DEFINE ANGLE ROTATIONS
```

Appendix A.3 Continued

```
C**   SIMPLE ROTATIONS

C**   ANGULAR VELOCITY

C**   POSITION VECTORS

C**   VELOCITIES


      IMPLICIT        DOUBLE PRECISION (A - Z)

      INTEGER         ILOOP, IPRINT, PRINTINT

      CHARACTER       MESSAGE(99)

      COMMON/LOOPVARS/ T

      COMMON/CONSTNTS/ ANAB1,ANAB2,BABO2,BW,F_D,HEIGHT

      COMMON/ALGBRAIC/
ANAC1,AOAC1,FOOT,KA3,FAB,FAB_A1,FAB_A2,FNA1,FNA2,

     &Q1,Q2,Q1p,Q1pp,L_TIBIA

      COMMON/MISCLLNS/ Pi,DEGtoRAD,RADtoDEG


C**   Open input and output files

      OPEN(UNIT=20, FILE='2dadult.in', STATUS='OLD')

      OPEN(UNIT=21, FILE='2dadult.1',  STATUS='UNKNOWN')

      OPEN(UNIT=22, FILE='2dadult.2',  STATUS='UNKNOWN')

      OPEN(UNIT=23, FILE='2dadult.3',  STATUS='UNKNOWN')

      OPEN(UNIT=24, FILE='2dadult.4',  STATUS='UNKNOWN')

      OPEN(UNIT=25, FILE='2dadult.5',  STATUS='UNKNOWN')

      OPEN(UNIT=26, FILE='2dadult.6',  STATUS='UNKNOWN')

      OPEN(UNIT=27, FILE='2dadult.7',  STATUS='UNKNOWN')
```

Appendix A.3 Continued

```
C**   Read top of input file
      READ(20,7000,END=7100,ERR=7101)

C**   Read values of constants from input file
      READ(20,7010,END=7100,ERR=7101) ANAB1,ANAB2,BABO2,BW,F_D,HEIGHT

C**   Write heading(s) to output file(s)
      WRITE(*, 6021)
      WRITE(21,6021)
      WRITE(22,6022)
      WRITE(23,6023)
      WRITE(24,6024)
      WRITE(25,6025)
      WRITE(26,6026)
      WRITE(27,6027)

C**   Unit conversions
      Pi       = 3.141592653589793D0
      DEGtoRAD = Pi/180.0
      RADtoDEG = 180.0/Pi

C**   Begin DO-loop(s)
      DO 4000  T = 0, 1.5D0, 0.01D0
C**   Evaluate output quantities
      CALL EQNS1()
```

Appendix A.3 Continued

```
      CALL IO()
4000  CONTINUE
       GOTO 5930
C**   Inform user of input and output filename(s)
5930  WRITE(*,6999)

6021  FORMAT('% FILE: 2dadult.1 ',/,'%',/,'%',7X,'T',13X,'Q1',13X,'Q2',/
     &,'%',4X,'(UNITS)',8X,'(UNITS)',8X,'(UNITS)',/)
6022  FORMAT('% FILE: 2dadult.2 ',/,'%',/,'%',7X,'T',12X,'FNA1',11X,'FNA
     &2',/,'%',4X,'(UNITS)',8X,'(UNITS)',8X,'(UNITS)',/)
6023  FORMAT('% FILE: 2dadult.3 ',/,'%',/,'%',7X,'T',13X,'FAB',10X,'FAB_
     &A1',9X,'FAB_A2',/,'%',4X,'(UNITS)',8X,'(UNITS)',8X,'(UNITS)',8X,'(
     &UNITS)',/)
6024  FORMAT('% FILE: 2dadult.4 ',/,'%',/,'%',7X,'T',11X,'FNA1/BW',8X,'F
     &NA2/BW',/,'%',4X,'(UNITS)',8X,'(UNITS)',8X,'(UNITS)',/)
6025  FORMAT('% FILE: 2dadult.5 ',/,'%',/,'%',7X,'T',11X,'FAB/BW',8X,'FA
     &B_A1/BW',6X,'FAB_A2/BW',/,'%',4X,'(UNITS)',8X,'(UNITS)',8X,'(UNITS
     &)',8X,'(UNITS)',/)
6026  FORMAT('% FILE: 2dadult.6 ',/,'%',/,'%',7X,'T',9X,'P_NO_AO[1]',5X,
     &'P_NO_AO[2]',5X,'P_NO_AO[3]',6X,'N_A[1,1]',7X,'N_A[1,2]',7X,'N_A[1
     &,3]',7X,'N_A[2,1]',7X,'N_A[2,2]',7X,'N_A[2,3]',7X,'N_A[3,1]',7X,'N
     &_A[3,2]',7X,'N_A[3,3]',/,'%',4X,'(UNITS)',8X,'(UNITS)',8X,'(UNITS)
     &',8X,'(UNITS)',8X,'(UNITS)',8X,'(UNITS)',8X,'(UNITS)',8X,'(UNITS)'
     &,8X,'(UNITS)',8X,'(UNITS)',8X,'(UNITS)',8X,'(UNITS)',8X,'(UNITS)',
```

Appendix A.3 Continued

```
 &/)
6027  FORMAT('% FILE: 2dadult.7 ',/,'%',/,'%',7X,'T',9X,'P_NO_BO[1]',5X,
    &'P_NO_BO[2]',5X,'P_NO_BO[3]',6X,'N_B[1,1]',7X,'N_B[1,2]',7X,'N_B[1
    &,3]',7X,'N_B[2,1]',7X,'N_B[2,2]',7X,'N_B[2,3]',7X,'N_B[3,1]',7X,'N
    &_B[3,2]',7X,'N_B[3,3]',/,'%',4X,'(UNITS)',8X,'(UNITS)',8X,'(UNITS)
    &',8X,'(UNITS)',8X,'(UNITS)',8X,'(UNITS)',8X,'(UNITS)',8X,'(UNITS)'
    &,8X,'(UNITS)',8X,'(UNITS)',8X,'(UNITS)',8X,'(UNITS)',8X,'(UNITS)',
    &/)
6999  FORMAT(//1X,'Input is in the file 2dadult.in',//1X,'Output is in t
    &he files 2dadult.i  (i=1, ..., 7)',//1X,'The output quantities and
    & associated files are listed in file 2dadult.dir',/)
7000  FORMAT(/////)
7010  FORMAT( 1000(59X,E30.0,/) )
      STOP
7100  WRITE(*,*) 'Premature end of file while reading 2dadult.in '
7101  WRITE(*,*) 'Error while reading file 2dadult.in'
      STOP
      END

C**********************************************************************
      SUBROUTINE      EQNS1()
      IMPLICIT        DOUBLE PRECISION (A - Z)
      COMMON/LOOPVARS/ T
      COMMON/CONSTNTS/ ANAB1,ANAB2,BABO2,BW,F_D,HEIGHT
```

Appendix A.3 Continued

```
            COMMON/ALGBRAIC/
ANAC1,AOAC1,FOOT,KA3,FAB,FAB_A1,FAB_A2,FNA1,FNA2,
     &Q1,Q2,Q1p,Q1pp,L_TIBIA
      COMMON/MISCLLNS/ Pi,DEGtoRAD,RADtoDEG


C**   Evaluate constants
      FOOT = 0.014D0*BW
      L_TIBIA = 0.233D0*HEIGHT
      ANAC1 = L_TIBIA
      AOAC1 = 0.57D0*ANAC1
      KA3 = 0.00468909276248725 7D0*BW*(ANAC1-AOAC1)**2

C**   Quantities which were specified
      Q1 = -1.05D0*T
      Q1p = -1.05D0
      Q1pp = 0
      Q2 = 1.675516081914556D0 - 0.2443460952792061D0*T

C**   Evaluate output quantities
      FNA1 = -FOOT*COS(Q1) - 0.04599999999999999D0*BW*COS(Q1) - 0.004689
     &092762487257D0*BW*(ANAC1-AOAC1)*Q1p**2 - 0.00468909276248725 7D0*SI
     &N(Q2)*(213.2608695652174D0*ANAC1*(F_D-FOOT*SIN(Q1))-9.810000000000
     &001D0*BW*(ANAC1-AOAC1)*SIN(Q1)-
(213.2608695652174D0*KA3+BW*(ANAC1-
     &AOAC1)**2)*Q1pp)/(ANAB1*COS(Q2)-ANAB2*SIN(Q2))
      FNA2 = FOOT*SIN(Q1) + 0.04599999999999999D0*BW*SIN(Q1) + 0.0046890
     &92762487257D0*BW*(ANAC1-AOAC1)*Q1pp +
0.00468909276248725 7D0*COS(Q
     &2)*(213.2608695652174D0*ANAC1*(F_D-FOOT*SIN(Q1))-9.810000000000001
     &D0*BW*(ANAC1-AOAC1)*SIN(Q1)-(213.2608695652174D0*KA3+BW*(ANAC1-
AOA
     &C1)**2)*Q1pp)/(ANAB1*COS(Q2)-ANAB2*SIN(Q2)) - F_D
```

Appendix A.3 Continued

```
FAB = -0.004689092762487257D0*(213.2608695652174D0*ANAC1*(F_D-FOOT
    &*SIN(Q1))-9.810000000000001D0*BW*(ANAC1-AOAC1)*SIN(Q1)-(213.260869
    &5652174D0*KA3+BW*(ANAC1-AOAC1)**2)*Q1pp)/(ANAB1*COS(Q2)-

ANAB2*SIN(
    &Q2))
     FAB_A1 = -SIN(Q2)*FAB
     FAB_A2 = COS(Q2)*FAB
     RETURN
     END

C**********************************************************************

     SUBROUTINE      IO()

     IMPLICIT        DOUBLE PRECISION (A - Z)

     INTEGER         ILOOP

     COMMON/LOOPVARS/ T

     COMMON/CONSTNTS/ ANAB1,ANAB2,BABO2,BW,F_D,HEIGHT

     COMMON/ALGBRAIC/
ANAC1,AOAC1,FOOT,KA3,FAB,FAB_A1,FAB_A2,FNA1,FNA2,

    &Q1,Q2,Q1p,Q1pp,L_TIBIA

     COMMON/MISCLLNS/ Pi,DEGtoRAD,RADtoDEG


C**   Write output to screen and to output file(s)

     WRITE(*, 6020) T,Q1,Q2

     WRITE(21,6020) T,Q1,Q2

     WRITE(22,6020) T,FNA1,FNA2

     WRITE(23,6020) T,FAB,FAB_A1,FAB_A2

     WRITE(24,6020) T,FNA1/BW,FNA2/BW

     WRITE(25,6020) T,FAB/BW,FAB_A1/BW,FAB_A2/BW

     WRITE(26,6020) T,((ANAC1-AOAC1)*COS(Q1)),((ANAC1-AOAC1)*SIN(Q1)),0
```

Appendix A.3 Continued

```
     &.0,COS(Q1),(-SIN(Q1)),0.0,SIN(Q1),COS(Q1),0.0,0.0,0.0,1.0D0
      WRITE(27,6020) T,(ANAB1*COS(Q1)+ANAB2*SIN(Q1)-BABO2*SIN(Q1+Q2)),(A
     &NAB1*SIN(Q1)+BABO2*COS(Q1+Q2)-ANAB2*COS(Q1)),0.0,COS(Q1+Q2),(-SIN(
     &Q1+Q2)),0.0,SIN(Q1+Q2),COS(Q1+Q2),0.0,0.0,0.0,1.0D0
6020  FORMAT( 99(1X, 1PE14.6E3) )
      RETURN
      END
```

A.4 Matlab code for the slow 13 year-old model.

```
_____________________________________________________________________________________________
**********************************************************************************************
function 13
% File  13.m  created by Autolev 4.0 on Thu Jan 29
18:43:58 2009
% MATHEMATICAL MODEL OF 13 Y/O YOUTH LEG EXTENSION
% 13_M.AL
% MATLAB OUTPUT
% ASSUMPTIONS: 2D
% LEFT LEG
% |
% |
% |
% |
% | N1>
%
% 3 AXIS ROTATIONS
% SIMPLE ROTATIONS
% ANGULAR VELOCITY
% POSITION VECTORS
% VELOCITIES

global   T;
global   ANAB1 ANAB2 BABO2 BW F_D HEIGHT;
global   ANAC1 AOAC1 FOOT KA3 FAB FAB_A1 FAB_A2 FNA1 FNA2
Q1 Q2 Q1p Q1pp L_TIBIA;
global   DEGtoRAD RADtoDEG;

OpenOutputFilesAndWriteHeadings

for T=0:  0.01:  1.5,
ReadUserInput;
DoCalculations;
PrintUserOutput;

end
CloseOutputFilesAndTerminate;
```

```
%==========================================================
==================
function ReadUserInput
global   T;
global   ANAB1 ANAB2 BABO2 BW F_D HEIGHT;
global   ANAC1 AOAC1 FOOT KA3 FAB FAB_A1 FAB_A2 FNA1 FNA2
Q1 Q2 Q1p Q1pp L_TIBIA;
global   DEGtoRAD RADtoDEG;
```

Appendix A.4 Continued

```
%------------------------------+------------------------
-+-------------------+-----------------
% Quantity                      | Value
| Units             | Description
%------------------------------|------------------------
-|-------------------|-----------------
ANAB1                           =  0.0294;
% UNITS               Constant
ANAB2                           =  0.0229;
% UNITS               Constant
BABO2                           =  0.137;
% UNITS               Constant
BW                              =  450;
% UNITS               Constant
F_D                             =  250;
% UNITS               Constant
HEIGHT                          =  1.56;
% UNITS               Constant
%------------------------------+------------------------
-+-------------------+-----------------

% Unit conversions
Pi       = 3.141592653589793;
DEGtoRAD = Pi/180.0;
RADtoDEG = 180.0/Pi;

% Evaluate constants
FOOT = 0.02065*BW;
L_TIBIA = 0.233*HEIGHT;
ANAC1 = L_TIBIA;
AOAC1 = 0.5964*ANAC1;
KA3 = 0.005504587155963302*BW*(ANAC1-AOAC1)^2;
```

```
%==========================================================
==================
function DoCalculations
global   T;
global   ANAB1 ANAB2 BABO2 BW F_D HEIGHT;
global   ANAC1 AOAC1 FOOT KA3 FAB FAB_A1 FAB_A2 FNA1 FNA2
Q1 Q2 Q1p Q1pp L_TIBIA;
global   DEGtoRAD RADtoDEG;

% Quantities which were specified
Q1 = -1.05*T;
Q1p = -1.05;
Q1pp = 0;
Q2 = 1.675516081914556 - 0.2443460952792061*T;
```

Appendix A.4 Continued

```
FNA1 = -FOOT*cos(Q1) - 0.054*BW*cos(Q1) -
0.005504587155963302*BW*(ANAC1-AOAC1)*Q1p^2 -
0.005504587155963302*sin(Q2)*(181.6666666666667*ANAC1*(F_D
-FOOT*sin(Q1))-9.810000000000001*BW*(ANAC1-AOAC1)*sin(Q1)-
(181.6666666666667*KA3+BW*(ANAC1-
AOAC1)^2)*Q1pp)/(ANAB1*cos(Q2)-ANAB2*sin(Q2));
FNA2 = FOOT*sin(Q1) + 0.054*BW*sin(Q1) +
0.005504587155963302*BW*(ANAC1-AOAC1)*Q1pp +
0.005504587155963302*cos(Q2)*(181.6666666666667*ANAC1*(F_D
-FOOT*sin(Q1))-9.810000000000001*BW*(ANAC1-AOAC1)*sin(Q1)-
(181.6666666666667*KA3+BW*(ANAC1-
AOAC1)^2)*Q1pp)/(ANAB1*cos(Q2)-ANAB2*sin(Q2)) - F_D;
FAB = -0.005504587155963302*(181.6666666666667*ANAC1*(F_D-
FOOT*sin(Q1))-9.810000000000001*BW*(ANAC1-AOAC1)*sin(Q1)-
(181.6666666666667*KA3+BW*(ANAC1-
AOAC1)^2)*Q1pp)/(ANAB1*cos(Q2)-ANAB2*sin(Q2));
FAB_A1 = -sin(Q2)*FAB;
FAB_A2 = cos(Q2)*FAB;




%==========================================================
==================
```

```
function Output = PrintUserOutput
global   T;
global   ANAB1 ANAB2 BABO2 BW F_D HEIGHT;
global   ANAC1 AOAC1 FOOT KA3 FAB FAB_A1 FAB_A2 FNA1 FNA2
Q1 Q2 Q1p Q1pp L_TIBIA;
global   DEGtoRAD RADtoDEG;

Output(1)=T;  Output(2)=Q1;  Output(3)=Q2;
Output(4)=T;  Output(5)=FNA1;  Output(6)=FNA2;
Output(7)=T;  Output(8)=FAB;  Output(9)=FAB_A1;
Output(10)=FAB_A2;
Output(11)=T;  Output(12)=FNA1/BW;  Output(13)=FNA2/BW;
Output(14)=T;  Output(15)=FAB/BW;  Output(16)=FAB_A1/BW;
Output(17)=FAB_A2/BW;
Output(18)=T;  Output(19)=((ANAC1-AOAC1)*cos(Q1));
Output(20)=((ANAC1-AOAC1)*sin(Q1));  Output(21)=0.0;
Output(22)=cos(Q1);  Output(23)=(-sin(Q1));
Output(24)=0.0;  Output(25)=sin(Q1);  Output(26)=cos(Q1);
Output(27)=0.0;  Output(28)=0.0;  Output(29)=0.0;
Output(30)=1.0;
Output(31)=T;  Output(32)=(ANAB1*cos(Q1)+ANAB2*sin(Q1)-
BABO2*sin(Q1+Q2));
Output(33)=(ANAB1*sin(Q1)+BABO2*cos(Q1+Q2)-ANAB2*cos(Q1));
Output(34)=0.0;  Output(35)=cos(Q1+Q2);  Output(36)=(-
sin(Q1+Q2));  Output(37)=0.0;  Output(38)=sin(Q1+Q2);
Output(39)=cos(Q1+Q2);  Output(40)=0.0;  Output(41)=0.0;
```

Appendix A.4 Continued

```
output(42)=0.0;  Output(43)=1.0;
FileIdentifier = fopen('all');
WriteOutput( 1,                Output(1:3) );
WriteOutput( FileIdentifier(1), Output(1:3) );
WriteOutput( FileIdentifier(2), Output(4:6) );
WriteOutput( FileIdentifier(3), Output(7:10) );
WriteOutput( FileIdentifier(4), Output(11:13) );
WriteOutput( FileIdentifier(5), Output(14:17) );
WriteOutput( FileIdentifier(6), Output(18:30) );
WriteOutput( FileIdentifier(7), Output(31:43) );



%=============================================================
=================
```

```
function WriteOutput( fileIdentifier, Output )
numberOfOutputQuantities = length( Output );
if numberOfOutputQuantities > 0,
  for i=1:numberOfOutputQuantities,
    fprintf( fileIdentifier, ' %- 14.6E', Output(i) );
  end
  fprintf( fileIdentifier, '\n' );
end


%============================================================
==================
function CloseOutputFilesAndTerminate
FileIdentifier = fopen('all');
fclose( FileIdentifier(1) );
fclose( FileIdentifier(2) );
fclose( FileIdentifier(3) );
fclose( FileIdentifier(4) );
fclose( FileIdentifier(5) );
fclose( FileIdentifier(6) );
fclose( FileIdentifier(7) );
fprintf( 1, '\n Output is in the files 13.i  (i=1, ...,
7)\n' );
fprintf( 1, ' The output quantities and associated files
are listed in the file 13.dir\n' );
fprintf( 1, '\n To load and plot columns 1 and 2 with a
solid line and columns 1 and 3 with a dashed line,
enter:\n' );
fprintf( 1, '    someName = load( ''13.1'' );\n' );
fprintf( 1, '    plot( someName(:,1), someName(:,2), ''-
'', someName(:,1), someName(:,3), ''--'' )\n\n' );
```

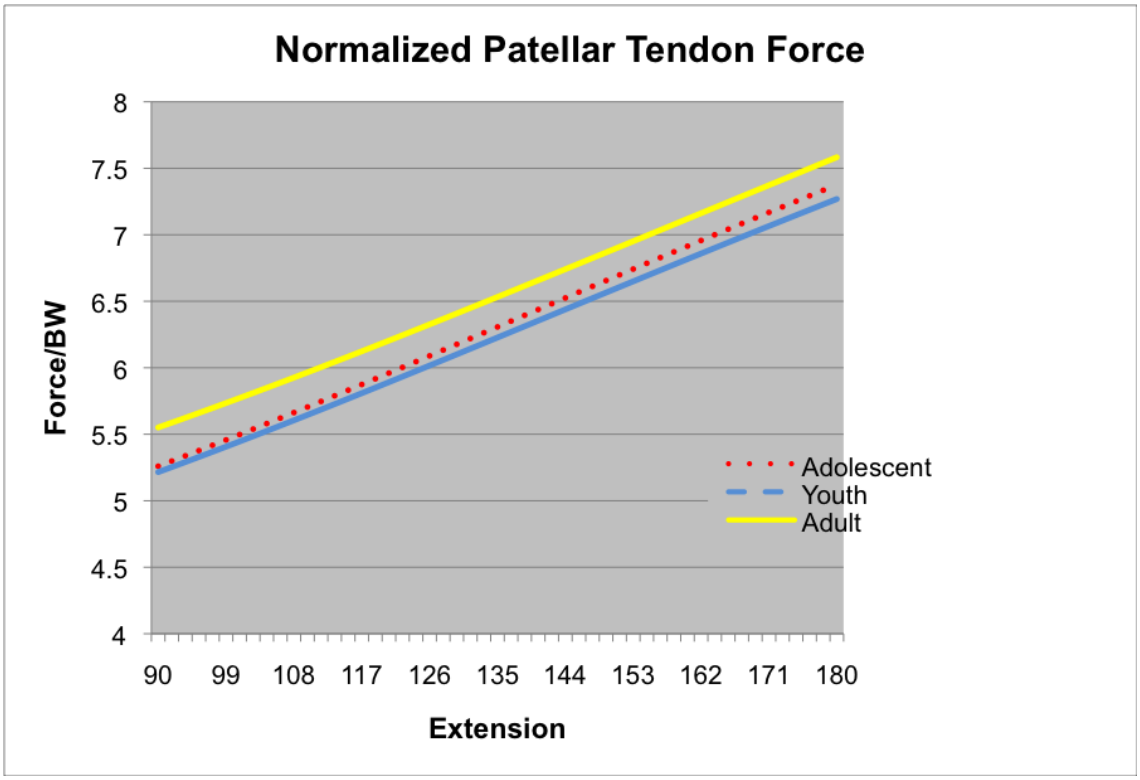

Figure 27. Age related changes in normalized patellar ligament force at 3.14 rad/s.

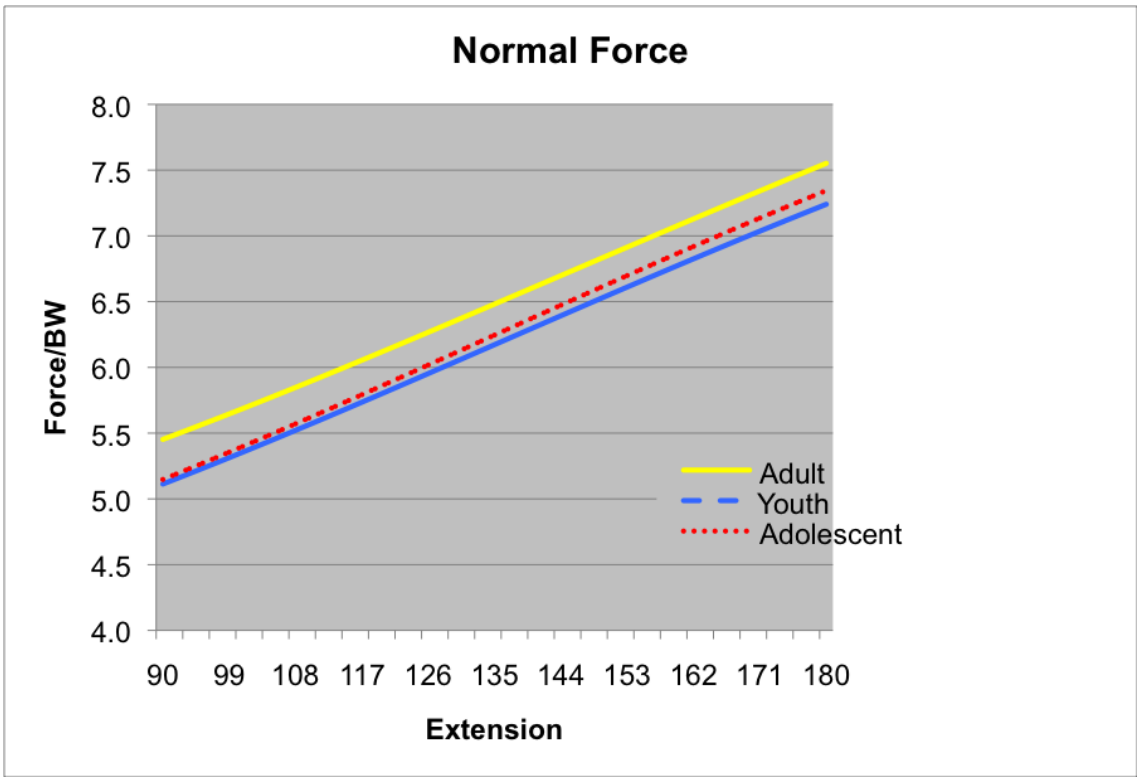

Figure 28. Age related changes in normalized femorotibial normal force at 3.14 rad/s.

Figure 29. Age related changes in normalized femorotibial shear force at 3.14 rad/s.

Table 7. Contents of 13_fast.2 - Normal and shear femorotibial forces for fast extension adolescent model.

% %	T (SEC)	FNA1 (N)	FNA2 (N)
	0.00	2310.16	79.09
	0.01	2344.20	63.22
	0.02	2378.85	46.92
	0.03	2414.07	30.19
	0.04	2449.84	13.01
	0.05	2486.13	-4.62
	0.06	2522.92	-22.71
	0.07	2560.18	-41.28
	0.08	2597.88	-60.31
	0.09	2635.99	-79.83
	0.10	2674.48	-99.83
	0.11	2713.33	-120.32
	0.12	2752.50	-141.31
	0.13	2791.96	-162.80
	0.14	2831.69	-184.79
	0.15	2871.65	-207.28
	0.16	2911.83	-230.28
	0.17	2952.19	-253.79
	0.18	2992.71	-277.80
	0.19	3033.36	-302.33
	0.20	3074.11	-327.37
	0.21	3114.96	-352.92
	0.22	3155.86	-378.99
	0.23	3196.82	-405.57
	0.24	3237.80	-432.66
	0.25	3278.79	-460.27
	0.26	3319.78	-488.40
	0.27	3360.75	-517.04
	0.28	3401.70	-546.20
	0.29	3442.62	-575.89
	0.30	3483.50	-606.10

Table 8. Contents of fast_grf.2 - Normal and shear femorotibial forces for jump take-off model.

% %	T (SEC)	FNA1 (N)	FNA2 (N)
	0.00	1306.43	0.00
	0.01	1275.59	-0.38
	0.02	1245.03	-0.95
	0.03	1214.74	-1.70
	0.04	1184.67	-2.65
	0.05	1154.78	-3.78
	0.06	1125.04	-5.10
	0.07	1095.41	-6.61
	0.08	1065.84	-8.30
	0.09	1036.30	-10.18
	0.10	1006.74	-12.23
	0.11	977.13	-14.45
	0.12	947.41	-16.83
	0.13	917.55	-19.38
	0.14	887.51	-22.07
	0.15	857.23	-24.90
	0.16	826.68	-27.86
	0.17	795.81	-30.93
	0.18	764.58	-34.12
	0.19	732.94	-37.39
	0.20	700.86	-40.74
	0.21	668.28	-44.15
	0.22	635.16	-47.61
	0.23	601.47	-51.10
	0.24	567.16	-54.61
	0.25	532.20	-58.10
	0.26	496.53	-61.57
	0.27	460.13	-65.00
	0.28	422.95	-68.35
	0.29	384.96	-71.63
	0.30	346.12	-74.79

Table 9. Contents of 13_fast.3 - Patellar tendon force for the fast extension model, separated into its components

% %	T (SEC)	FAB (N)	FAB_A1 (N)	FAB_A2 (N)
	0.00	2366.70	-2353.73	-247.39
	0.01	2399.10	-2387.73	-233.28
	0.02	2432.09	-2422.23	-218.74
	0.03	2465.65	-2457.22	-203.75
	0.04	2499.77	-2492.67	-188.30
	0.05	2534.42	-2528.56	-172.38
	0.06	2569.58	-2564.85	-155.97
	0.07	2605.23	-2601.52	-139.07
	0.08	2641.35	-2638.54	-121.66
	0.09	2677.90	-2675.89	-103.73
	0.10	2714.89	-2713.55	-85.28
	0.11	2752.27	-2751.47	-66.28
	0.12	2790.03	-2789.64	-46.75
	0.13	2828.16	-2828.03	-26.65
	0.14	2866.62	-2866.62	-6.00
	0.15	2905.41	-2905.37	15.21
	0.16	2944.50	-2944.27	37.00
	0.17	2983.88	-2983.29	59.37
	0.18	3023.53	-3022.41	82.31
	0.19	3063.44	-3061.61	105.84
	0.20	3103.59	-3100.86	129.96
	0.21	3143.97	-3140.16	154.68
	0.22	3184.57	-3179.48	179.99
	0.23	3225.38	-3218.80	205.89
	0.24	3266.40	-3258.12	232.40
	0.25	3307.62	-3297.43	259.51
	0.26	3349.04	-3336.70	287.23
	0.27	3390.66	-3375.95	315.55
	0.28	3432.48	-3415.15	344.49
	0.29	3474.51	-3454.31	374.04
	0.30	3516.75	-3493.44	404.20

Table 10. Contents of fast_grf.3 - Patellar tendon force for jump take-off model, separated into components.

% %	T (SEC)	FAB (N)	FAB_A1 (N)	FAB_A2 (N)
	0.00	0.00	0.00	0.00
	0.01	14.18	-14.11	-1.38
	0.02	28.53	-28.42	-2.57
	0.03	43.04	-42.90	-3.56
	0.04	57.67	-57.50	-4.34
	0.05	72.37	-72.20	-4.92
	0.06	87.12	-86.96	-5.29
	0.07	101.89	-101.74	-5.44
	0.08	116.62	-116.50	-5.37
	0.09	131.30	-131.20	-5.09
	0.10	145.88	-145.80	-4.58
	0.11	160.32	-160.27	-3.86
	0.12	174.58	-174.56	-2.93
	0.13	188.64	-188.63	-1.78
	0.14	202.44	-202.44	-0.42
	0.15	215.95	-215.95	1.13
	0.16	229.14	-229.12	2.88
	0.17	241.96	-241.91	4.81
	0.18	254.38	-254.28	6.93
	0.19	266.35	-266.20	9.20
	0.20	277.85	-277.61	11.64
	0.21	288.83	-288.48	14.21
	0.22	299.26	-298.78	16.91
	0.23	309.09	-308.46	19.73
	0.24	318.30	-317.49	22.65
	0.25	326.84	-325.84	25.64
	0.26	334.69	-333.46	28.70
	0.27	341.81	-340.32	31.81
	0.28	348.16	-346.40	34.94
	0.29	353.71	-351.65	38.08
	0.30	358.43	-356.05	41.20

Appendix B. Abaqus Contour Images

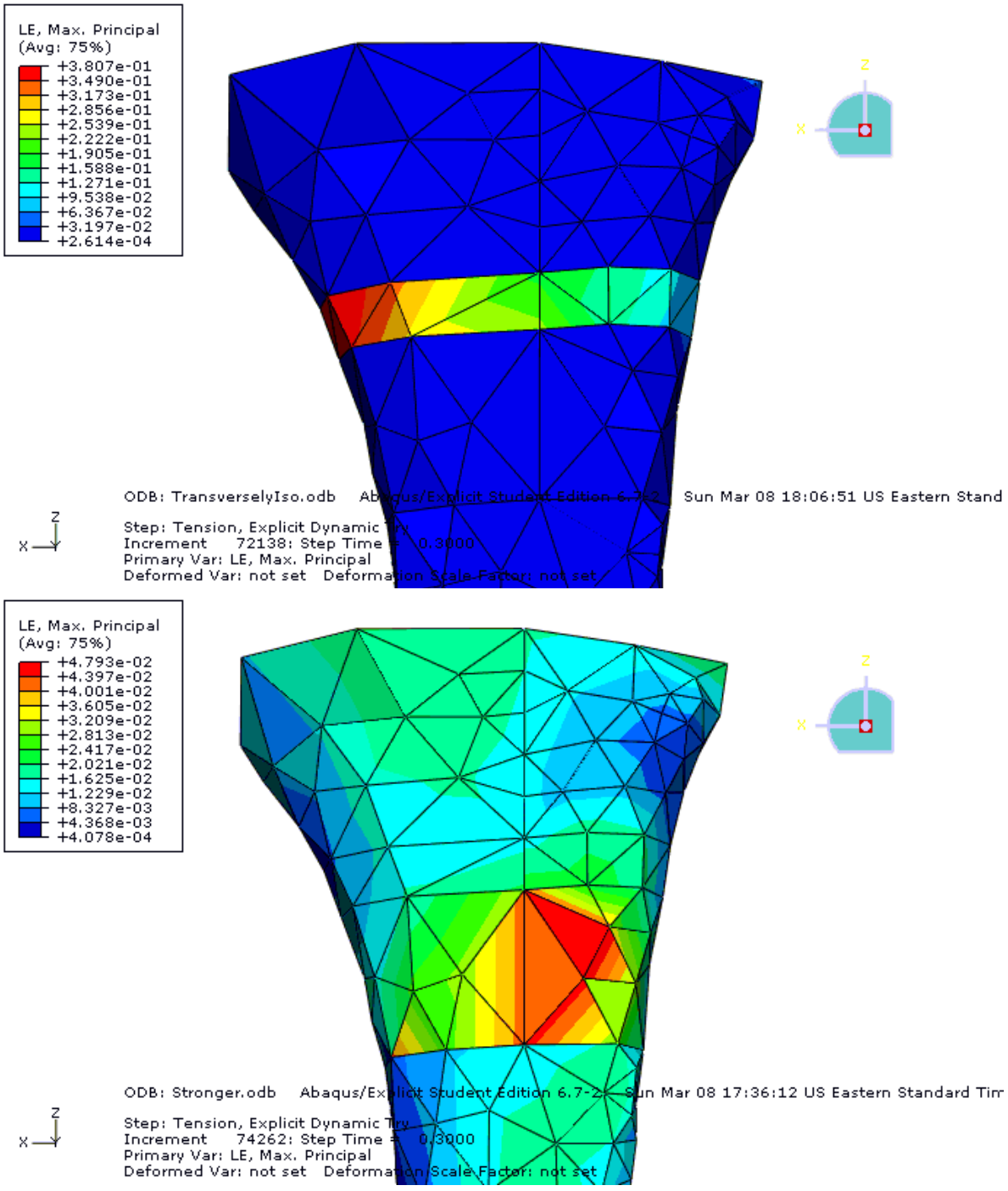

Figure 30. Anterior strain in the transversely isotropic growth plate model (top) and stronger material model.

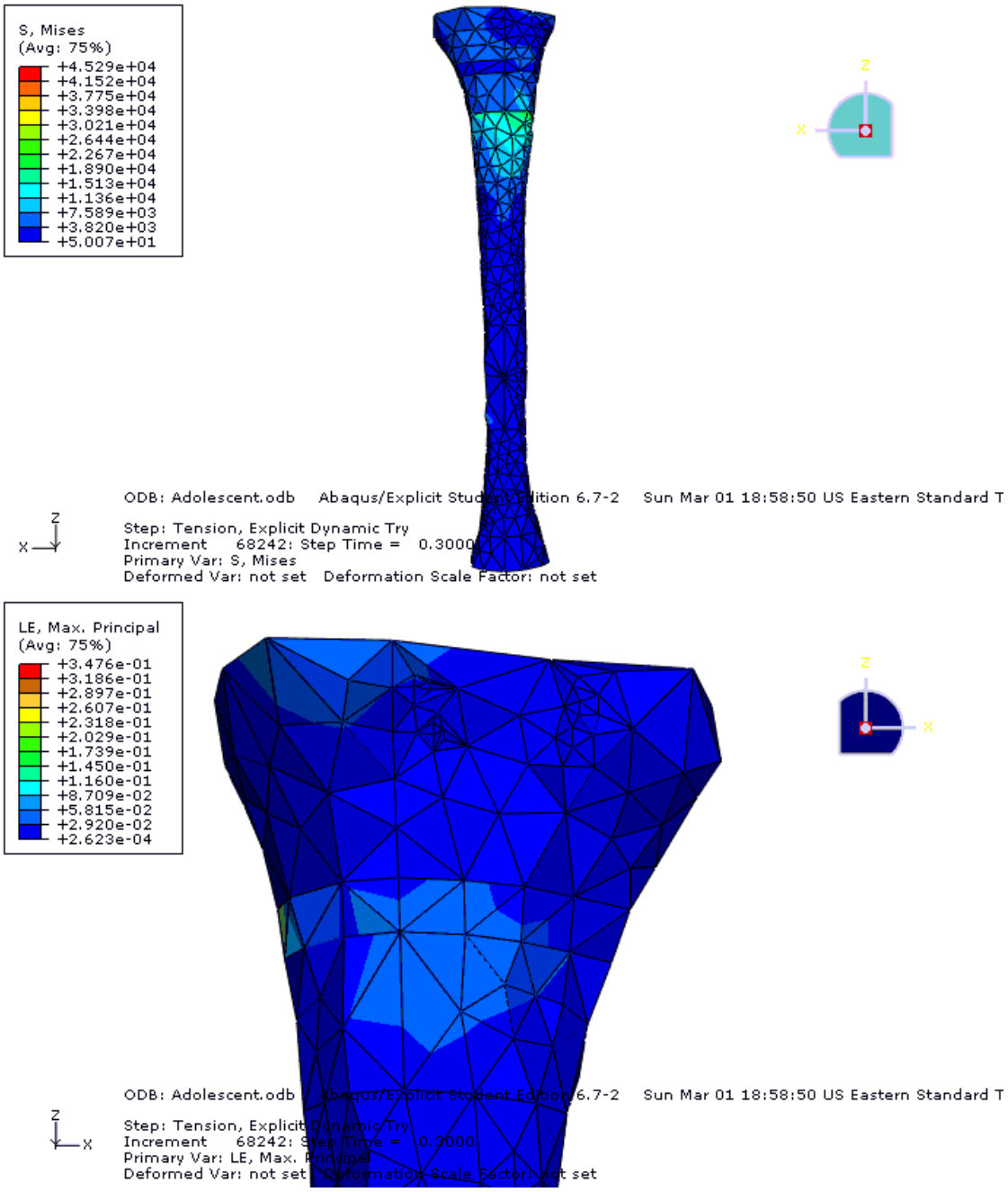

Figure 31. Viscoelastic model anterior stress (top) and posterior strain.

VITA

Susan Basile was born on February 17th, 1985 in Brooklyn, New York to Deila and Lawrence Basile. She has a younger brother, James. In 2003, Susan graduated valedictorian from The Mary Louis Academy in Jamaica, Queens. Upon completing her secondary education, she enrolled in the Columbia University School of Engineering and Applied Science. In 2007, Susan graduated with a Bachelor of Science in biomedical engineering, with a concentration in biomechanics and a minor in economics. She then decided to continue her education at the University of Tennessee, Knoxville. In the fall of 2007, Susan began her graduate studies in biomedical engineering with emphasis in biomechanics, and was supported by a generous fellowship from the Pipeline Engineering Diversity program. She intends to continue her study and research on the musculoskeletal biomechanics of athletics, youth, injury, and rehabilitation.